X-RAY PHOTOELECTRON SPECTROSCOPIC INVESTIGATION OF GOLD PARTICLES DEPOSITED ON SiO_2/Si SYSTEM

A THESIS
SUBMITTED TO THE DEPARTMENT OF CHEMISTRY
AND THE INSTITUTE OF ENGINEERING AND SCIENCES
OF B□LKENT UNIVERSITY
IN PARTIAL FULFILLMENT OF THE REQUIREMENTS
FOR THE DEGREE OF
MASTER OF SCIENCE

By
FERD□ KARADA□
July 2003

I certify that I have read this thesis and that in my opinion is it is fully adequate, in scope and quality, as a thesis of the degree of Master in Science

……..

Prof. Dr. □efik Süzer (Principal Advisor)

I certify that I have read this thesis and that in my opinion is it is fully adequate, in scope and quality, as a thesis of the degree of Master in Science

……..

Prof. Dr. O. Yavuz Ataman

I certify that I have read this thesis and that in my opinion is it is fully adequate, in scope and quality, as a thesis of the degree of Master in Science

……..

Assoc. Prof. Dr. Ömer Da□

I certify that I have read this thesis and that in my opinion is it is fully adequate, in scope and quality, as a thesis of the degree of Master in Science

……..

Assoc. Prof. Dr. Margarita Kantcheva

I certify that I have read this thesis and that in my opinion is it is fully adequate, in scope and quality, as a thesis of the degree of Master in Science

……..

Assoc. Prof. Dr. Ahmet Oral

Approved for the Institute of Engineering and Sciences

……..

Prof. Dr. Mehmet Baray

Director of Institute of Engineering and Science

ABSTRACT

X-RAY PHOTOELECTRON SPECTROSCOPIC INVESTIGATION OF GOLD PARTICLES DEPOSITED ON SiO_2/Si SYSTEM

FERD□KARADA□

M.S. in Chemistry

Supervisor: Prof. Dr. □efik Süzer

July, 2003

Gold particles on SiO_2/Si system were investigated by X-ray Photoelectron Spectroscopy (XPS) technique. A suitable reference point was first established in order to investigate the physical/chemical factors affecting chemical shift of gold particles. Gold particles were: i) deposited directly from aqueous solution, ii) capped with citrate agent and then deposited, iii) reduced chemically by $NaBH_4$ and deposited on SiO_2/Si system. In addition, gold particles were deposited onto different substrates (quartz, glass).

Similar chemical shift of Si^{4+} 2p and Au^0 4f peak upon the application of external bias gave a strong evidence to the assumption that SiO_2 could be chosen as reference. In addition, the derived Auger Parameters have shown that chemical shifts observed during the application of external bias are solely due to charging.

It was shown that reduction and nucleation processes occur at the same time during X-ray exposure when gold particles are deposited from aqueous solution. Differential charging of gold particles was investigated by measuring the changes in: i) binding energy, ii) FWHM and iii) intensity values of Au^0 and Si^{4+} peaks. Our findings obtained from Angle Resolved XPS method supported the assumption that gold particles deposited from aqueous solution prefer to grow three-dimensionally.

Assuming the Si 2p binding energy of Si^{4+} peak as a reference, the binding energy of gold particles is: i) 84.30 ± 0.05 eV when gold is deposited from aqueous solution, ii)

84.00 ± 0.05 when citrate capped gold particles are used, iii) 84.10 ± 0.05 when gold is chemically reduced by $NaBH_4$.

Vis-absorption and electrophoresis methods have shown that capped gold particles have negative charges and they aggregate reversibly (i.e. without coagulation) when they are deposited on SiO_2/Si system from their aqueous solution (and transferred back).

Keywords: Gold, SiO_2/Si, XPS, charging, Angle Resolved XPS, Application of an External Bias, Auger Parameter, Citrate Capping, Reduction, Nucleation.

ÖZET

SiO_2/Si NUMUNESİ ÜZERİNE DEPOLANAN ALTIN PARÇACIKLARININ X-IŞINI FOTOELEKTRON SPEKTROSKOPİSİ YÖNTEMİYLE İNCELENMESİ

FERDİ KARADAŞ

Kimya Bölümü Yüksek Lisans Tezi

Tez Yöneticisi: Prof. Dr. Şefik Süzer

Temmuz 2003

SiO_2/Si numunesi üzerine depolanan altın parçacıkları X-ışınlı Fotoelektron Spektroskopisi (XPS) yöntemi ile incelendi. Altına ait tepede meydana gelen kimyasal kaymaya sebep olan fiziksel/kimyasal etkenleri araştırmak için uygun bir referans noktası tespit edilmeye çalışıldı. Altın parçacıklar; i) Au^{3+} sulu çözeltisi kullanılarak doğrudan, ii) sitrat bileşiğiyle kaplandıktan sonra, iii) $NaBH_4$ ile kimyasal olarak indirgendikten sonra SiO_2/Si üzerinde depolandı. Ayrıca, altın parçacıklar farklı numuneler üzerinde depolandı (cam, kuvars).

Numuneye dışarıdan voltaj uygulanmasıyla Si^{4+} 2p ile Au^0 4f tepelerinin benzer kaymalar göstermesi SiO_2 tabakasının referans olarak kullanılabileceğini gösterdi. Hesaplanan Auger parametreleri ve dışarıdan voltaj uygulanmasıyla Si^{4+} tepesinde meydana gelen kaymanın tamamiyle yük birikiminden kaynaklandığını gösterdi.

Altın parçacıkların sulu çözeltiden depolanıp, X-ışınlarına maruz bırakılması sonucu indirgenme ve parçacıkların büyümesi işlemlerinin birlikte meydana geldiği tespit edildi. Bunun yanısıra, altın parçacıklar üzerindeki diferansiyel yük birikimi, Au^0 ile Si^{4+} tepelerinin; i) bağlanma enerjileri, ii) FWHM değerleri, ve iii) şiddetleri kıyaslanarak araştırılmıştır. Açıya bağlı XPS yöntemi ile altın parçacıklarının üç-boyutlu büyümeyi tercih ettiğini gösteren veriler elde edildi.

SiO_2 tabakasının Si 2p tepesinin referans olarak alındığında, Au^0 tepesinin bağlanma enerjisi; i) sulu çözeltiden depolanan altın parçacıklar için 84.30 ± 0.05 eV, ii) sitrat kaplı altın parçacıklar için 84.00 ± 0.05 eV, iii) $NaBH_4$ ile kimyasal olarak indirgenerek elde edilen altın parçacıklar için 84.10 ± 0.05 eV olarak tespit edildi.

Görünür bölge soğurma bandlarının takibi ve elektroforez yöntemi ise sitrat kaplı altın parçacıklarının eksi yüke sahip olduklarını ve SiO_2/Si numunesi üzerinde depolanıp tekrar çözeltiye alındığında, tersinir bir şekilde toplandıklarını –photobleaching olmadığını– gösterdi.

Anahtar Kelimeler: Altın, SiO_2/Si, XPS, Yük Birikimi, Açıya Bağlı XPS, Dışarıdan Voltaj Uygulama Yöntemi, Auger Parametresi, Sitrat Kaplaması, İndirgenme, Büyüme.

ACKNOWLEDGEMENTS

I would like to express my deepest gratitude to Prof. Dr. Çefik Süzer for his leadership and supervision throughout my studies.

I would like to give my heartfelt thanks to Dr. Gülay Ertaş for her encouragement and discussions during the research.

My thanks also go to Ercan Avcı, H. Nezih Türkçü, Burak Ulgut, Sinan Balcı, U. Korcan Demirok for their help in the lab.

I appreciate the moral support by dear friends; Ozan Karaltı, Serdar Durdağı, İshak Uysal, Cenk Tura, İlknur Tunç, Işık R. Türkmen, Banu Altıntaş, Tuba Özal and Olga Samarskaya. I am also grateful to Yasemur Yılmaz, Salih Özçubukçu, Cafer T. Yavuz, Murat Kaya and Serap Tekin for their endless help and friendship.

I would like to express my deepest gratitude to my family for their moral support and encouragement.

TABLE OF CONTENTS

LIST OF TABLES

LIST OF FIGURES

1. INTRODUCTION

1.1 Metal-Oxide-Semiconductor Systems

Due to continuous progress in microelectronics industry for approximately thirty years, MOS (metal-oxide-semiconductor) technology has received great attention since it has been observed that these devices behave as both capacitors and transistors according to the applied potential to the substrate [1]. Studies on different systems have been made in order to find the most suitable combination for this trilayer system. Although Ge was the first element used as semiconductor, today 98% of electronic industry production is based on silicon. Furthermore, it is well known that SiO_2/Si substrate is the most appropriate substrate to use for oxide-semiconductor systems in MOS-devices because of both its easy preparation and stability against many reactants. SiO_2/Si system was chosen because of its advantages over Ge, listed below;

- Si crystal has a relatively wider band gap (1.1 eV) than Ge (0.7 eV). This difference results in that Si-devices can operate up to 150 ^oC whereas devices made up of germanium can operate only up to 100 ^oC. Another result is that silicon has a higher resistivity ($2.3*10^5$ ohm.cm) than germanium (47 ohm.cm).

- In addition to the easy preparation of SiO_2 layer, it can be easily cleaned by HF solution which has a good etching selectivity between SiO_2 and Si as shown in Figure 1.

- SiO_2 is suitable for planar processing technology and is electrically insulator (band gap is 9.65 eV).

- SiO_2 is a good diffusion mask for common dopants such as B, P, As and Sb.

Considering that MOS systems consisting of SiO_2/Si substrates have found application in various fields such as optoelectronics, nanodevices, catalysis and chemical

sensors besides their use in microelectronics industry, different physical and chemical properties of SiO_2/Si substrate have been investigated in numerous studies [2-11].

Growth of a uniform thin oxide layer could be managed by thermal oxidation of Si wafer as shown in Figure 1. Although silicon oxide could form different crystalline structures such as quartz, tridymite and cristobalite, amorphous silicon oxide layer is obtained by thermal oxidation where tetrahedral blocks, involving SiO_4 units, form a continuous random network [1,12].

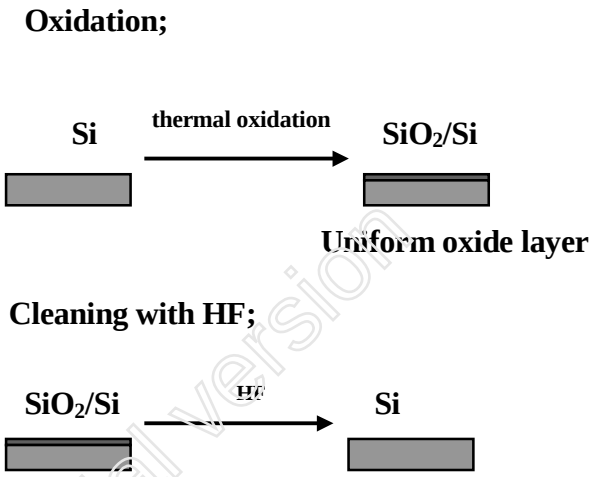

Figure 1. Preparation and cleaning procedure for SiO_2 layer on Si wafer

Covering the SiO_2/Si substrate with a metallic layer, one obtains a MOS system. Metals, which are unreactive to oxidation reactions, are preferred for MOS system. Gold is one of the metals suitable for this purpose. Gold is known as one of the most stable elements among noble metals with respect to oxidation reactions and to oxygen at elevated temperatures. Especially due to its increasing importance in catalysis, several studies have been performed dealing with gold nanoparticles deposited on oxides such as TiO_2, SiO_2, Al_2O_3 [1-15]. In this thesis, gold particles on SiO_2(1-10 nm)/Si substrate are investigated.

Being one of the noble metals, gold prefers to be in its metallic state and it is stable in water. Positive reduction potential of Au^{3+} to its metallic state (1.5 V), also proves this stability. In addition to +3 state, +1 state could also be formed with larger anions such as bromide and iodide or with π-acceptor ligands such as PPh_3 that stabilizes Au(I) [16,17].

Gold metal has cubic closed-packed crystal structure having a lattice constant of 407.8 pm. In Table 1 below, some properties of gold, silicon oxide and silicon are shown to give brief information about their bulk properties.

Table 1. Data for Au, SiO_2 and Si

	Gold	**SiO_2**	**Si**
Structure	Cubic	Amorphous	Cubic
Density (gr/cm^3) [18]	19.32	2.2	2.33
Atomic density (cm^{-3})	0.0978	0.0377	0.083
Conductivity (ohm.cm)$^{-1}$	$5*10^7$ conductor	$1*10^{-18}$ insulator	$4*10^{-5}$ semiconductor

Today's MOS technology allows the preparation of systems having a layer thickness of about 100 nanometers [19,20]. However, studies devoted to MOS systems are aimed to prepare systems with 5-10 nanometer thickness to decrease the size dimensions in the new future. For this purpose, instruments sensitive to the surface properties are used to investigate MOS systems such as secondary ion mass spectroscopy (SIMS), X-ray Photoelectron Spectroscopy (XPS), Auger Photoelectron Spectroscopy, Atomic Force Microscopy (AFM), Scanning Tunneling Microscopy (STM), etc. XPS is used in this research.

1.2 X-ray Photoelectron Spectroscopy

X-ray Photoelectron Spectroscopy, so-called XPS, is one of the most powerful methods for surface analysis of solids, thin films and nanostructures. Surface analysis simply deals the determination of the elemental composition of the outermost atom layers of materials. With a more detailed analysis, information about the chemical binding state and precise sites of atoms in the crystal structure, surface homogeneity and the state of adsorbates can be obtained [21].

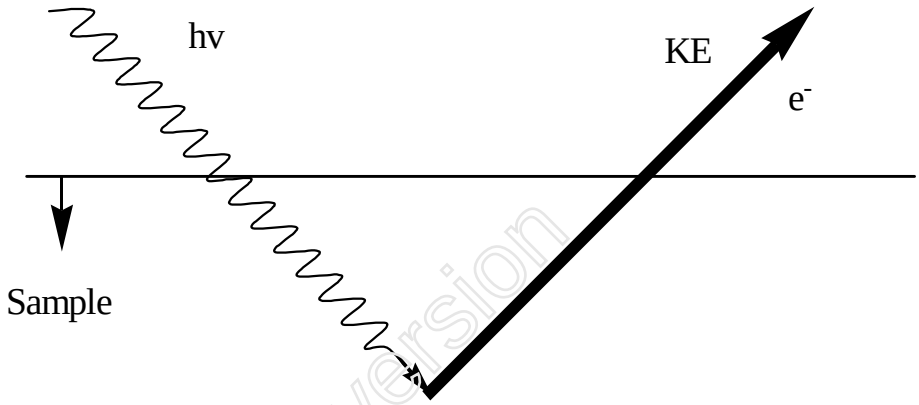

Figure 2. Classical representation of the creation of a photoelectron

The main logic of XPS is that, when a sample is subjected to X-rays having energy greater or equal to the binding energy of an electron bound in the atom, a free electron, the so-called the photoelectron, is emitted according to the Einstein relation stated below;

$$BE = h\nu - KE \qquad (1)$$

where BE is the binding energy of the electron, hν corresponds to the X-ray energy and KE is the kinetic energy of the ejected (and detected) photoelectron. Representation of equation (1) is shown in Figure 2.

Since photoelectrons interact strongly with the atoms around them due to their negative charges, ultrahigh vacuum system ($<10^{-8}$ torr) is needed in order to detect a substantial portion of them. In addition, because electrons interact with the atoms of the sample during the emission process, electrons, which are created near the surface, will have greater chance to get out of the sample. As photoelectrons move through the sample, they suffer of energy loss as a result of inelastic scatterings with atoms of the sample. The sensitivity of the sample to photoelectrons can be determined by a term called *inelastic mean free path* (λ). The electron inelastic mean free path (IMFP) is the average distance, measured along the trajectories that a particle with a given energy travels between successive inelastic collisions in a substance. Because electrons emitted from deeper part of the sample will lose considerable portion of energy, they will not be able to reach the detector. Electrons can travel only a distance of 3λ through the sample without any significant energy loss. Accordingly, photoelectrons emitted from atoms close to surface (<10 nm) reach the detector since the mean free path has a small value ranging from 2 to 4 nanometers for different atoms and electrons. This is why XPS is a surface sensitive technique. Using this technique, one can investigate basically:

- the binding energy (obtained from the kinetic energy)
- intensity
- angular dependence

of the electrons emitted from the sample.

1.2.1 Binding Energy of an Electron

The energy of the X-rays is known and kinetic energy of photoelectrons is measured with the electron-energy analyzer. Using these data, a spectrum, intensity versus the binding energy, can be plotted as shown in Figure 3. Then, chemical analysis of a sample can be made with binding energies obtained from the XPS-spectrum of the sample. In other words, qualitative and chemical state information are obtained. As an example, when Figure 3 is evaluated, one can conclude that sample surface (<10 nm) contains Cl, Si and Au atoms. Furthermore, it can be said that Si atoms in the sample have 0 and +4 oxidation states since XPS gives information about the oxidation states of atoms.

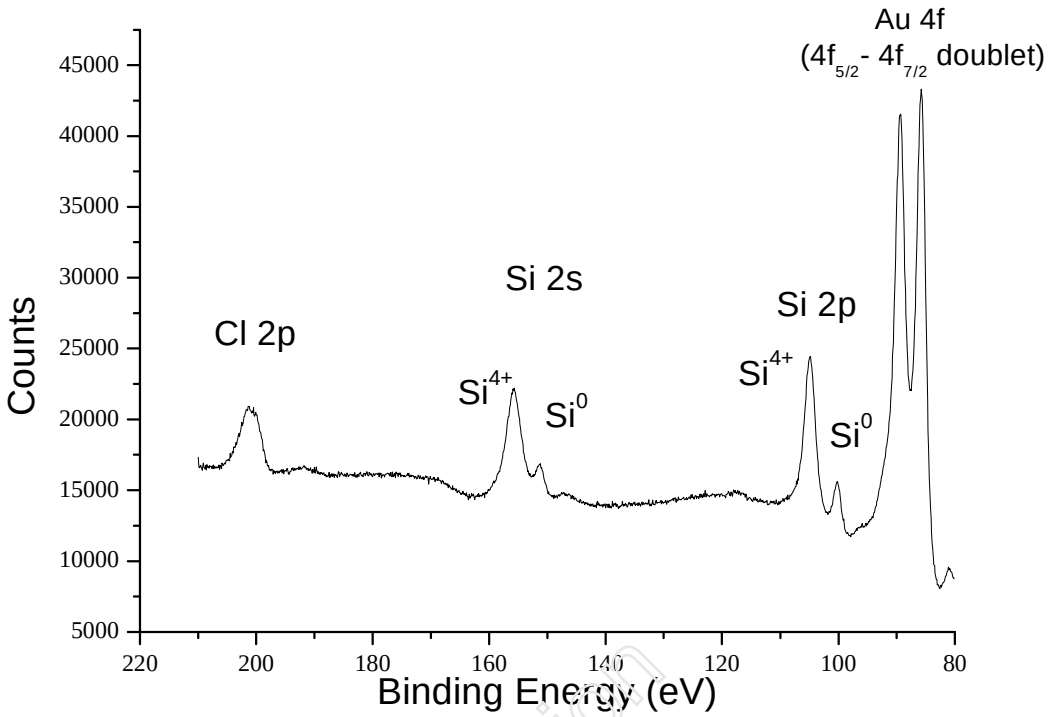

Figure 3. A typical XPS spectrum (this work)

Electrons emitted from the 2p orbital of Si and Si^{4+} atoms have a binding energy difference of approximately 4 eV (99.5 eV for Si, 103.5 eV for Si^{4+}). Another point is that all electrons emitted from non-s subshells (p,d,f) end up in doublets due spin-orbit interaction as given in Table 2 [21,22].

Table 2. Spin-orbit-splitting values for some levels [19,23]

Level	Spin orbit splitting value (eV)	j-values	Peak ratio (2j + 1)
Si 2p	0.607	3/2, 1/2	2:1
Cl 2p	1.60	3/2, 1/2	2:1
Au 4f	3.67	5/2, 3/2	3:2

1.2.2 Intensity Measurement

The intensity of the peaks give explicit data about the ratio of the atoms in the sample described by the formula [21];

$$\frac{[C]_A}{[C]_B} = \frac{A_A}{A_B}\frac{\sigma_B}{\sigma_A}\left(\frac{E_K^B}{E_K^A}\right)^{3/2} \quad (2)$$

where A is the area of the corresponding peak in the spectrum, σ is the photoionization cross-section of the atom, and E_K is the kinetic energy of the photoelectron emitted from the corresponding atom.

1.2.3 Angle Resolved XPS

Surface sensitivity of XPS technique can be further enhanced down to 1-2 nm levels by reducing the take-off angle of the photoelectrons. This is also useful for determining the thicknesses of the layers and extracting information about the distribution of various atoms/clusters within different overlayers [24,33]. For a bilayer system as shown in Figure 4, relations 3 and 4 can be derived;

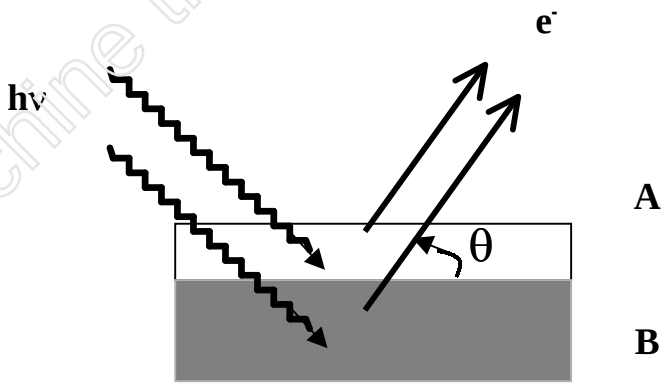

Figure 4. Two-layer system with an overlayer thickness d

$$\frac{I_A}{I_A^{\infty}} = 1 - \exp\left(-\frac{d}{\lambda_{AA}^{\infty} Sin\theta}\right) \tag{3}$$

$$\frac{I_B}{I_B^{\infty}} = \exp\left(-\frac{d}{\lambda_{BA}^{\infty} Sin\theta}\right) \tag{4}$$

where I_A^{∞} and I_B^{∞} are the intensities for the bulk materials, d is the thickness of the overlayer A, θ is the take-off angle, λ_{AA}^{∞} is the attenuation length of A electrons in A and λ_{BA}^{∞} is the attenuation length of B electrons in A. In order to obtain these expressions, two assumptions are made;

- Layers are perfectly smooth.
- The bottom layer B is infinitely thick.

When one divides equation 3 with 4, equation 5 will be obtained.

$$\frac{I_B}{I_A} = K \frac{1 - \exp\left(-\frac{d}{\lambda_B Sin\theta}\right)}{\exp\left(-\frac{d}{\lambda_A Sin\theta}\right)} \tag{5}$$

where K is formulated as [33];

$$K = \frac{n_B \sigma_B \lambda_B}{n_A \sigma_A \lambda_A} \tag{6}$$

where n is the atomic density, σ is the photoionization cross-section.

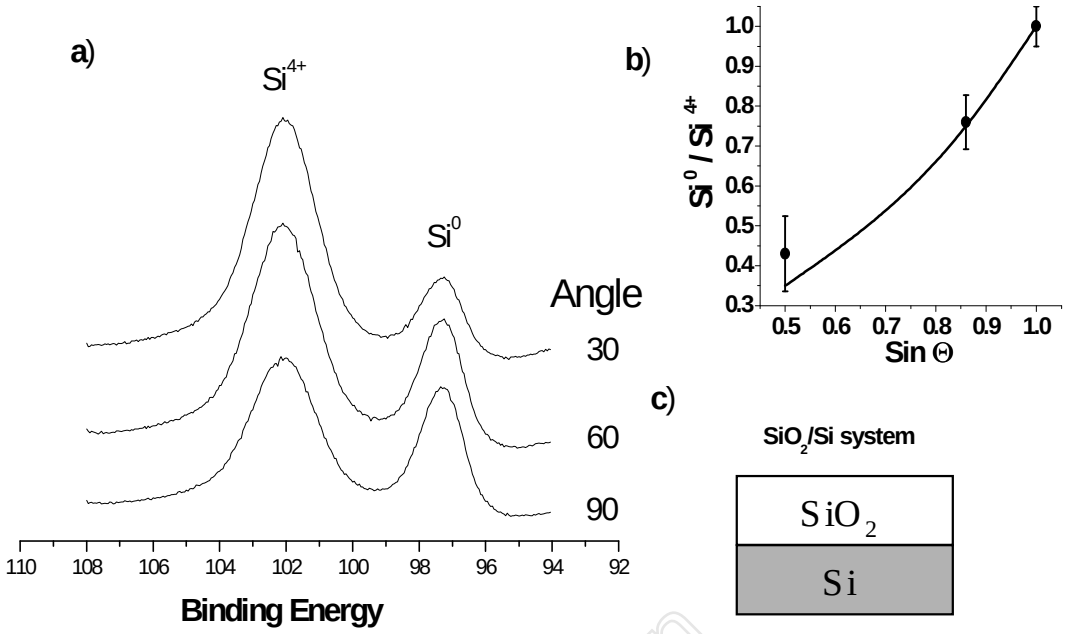

Figure 5. a) X-ray photoelectron spectrum of SiO_2/Si substrate at different take-off angles, **b)** Si^0 / Si^{4+} peak intensity ratio vs sin θ (solid line is theoretical plot), **c)** Structure of SiO_2/Si system

As a simple model, SiO_2/Si substrate can be used. As seen in Figure 5.a) and 5.b), by decreasing the take-off angle, Si peak decreases substantially relative to Si^{4+} peak. As the take-off angle is decreased, trajectory of electrons in the sample increases since the path distance of electrons is related to 'd/sinθ'. This causes photoelectrons emitted from atoms closer to sample surface to increase compared to those emitted from deeper part of the sample. Considering this situation, the structure of SiO_2/Si substrate can be illustrated as shown in Figure 5.c).

1.3 Measurement of Binding Energy with XPS

Since the kinetic energy of electrons can easily be influenced by many instrumental effects, each spectrum must be calibrated with respect to standards. Although there were remarkable differences among the results of energy calibration values earlier, today

calibration procedure is more straightforward [21,34-37]. For XPS instrument, energy scales have been calibrated according to Cu $2p_{3/2}$ and Au $4f_{7/2}$ peaks for several peaks. When nickel is used as referenceand the valence band of Ni atom is assumed at the Fermi level, Au $4f_{7/2}$ peak was measured at 83.98 ± 0.02 eV for Al Kα source and 84.00 ± 0.01 eV for Mg Kα source [38]. However, there usually occurs a shift from 84 eV as a result of various factors. This shift is called *chemical shift.* Important characteristic properties of the analyzed atom can be obtained using chemical shifts. A chemical shift measured in a sample may be the result of several factors or combination of them. These factors can be classified in two groups;

- *Initial-state effects*; which consist of factors that changes the core electron energy levels prior to photoemission process,

- *Final-state effects*; which consist of factors resulting in changes to stabilize the system after photoemission process.

In addition, there is one more factor called *charging effect,* accompanying the photoemission process, which results as measured chemical shift. All these three effects are explained briefly below;

1.3.1 Initial State Effects

These effects involve the factors that influence the atomic energy levels of the element before the photoelectron is emitted. Basically the changes in the compositional and structural features of the atom contribute to initial state effects.

1.3.1.1 Oxidation State of the Atom

Using XPS technique, same atoms with different oxidation states can be differentiated. As an example, binding energy values for silicon 2p level with different oxidation states are tabulated in Table 3. As the oxidation state of silicon goes to more positive values, binding energy increases proportionally. As shown in Figure 6, Si 2p peaks appears as well separated two peaks corresponding to SiO_2 and Si.

Table 3. Si 2p binding energy value for different silicon compounds [21,23]

Species	Binding energy (eV)
Silicon	98.8 - 99.5
Carbides	99.9 - 100.9
Nitrides	101.5 - 102.2
Siloxanes	101.9 - 102.8
Oxides (Silica)	103.2 - 103.8

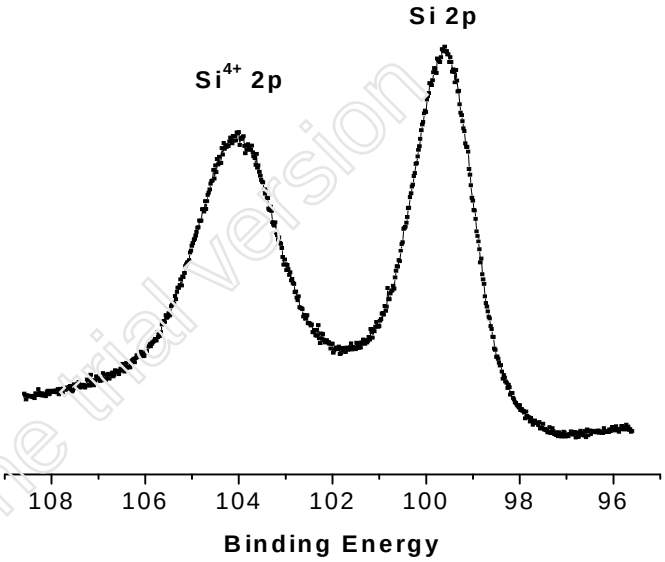

Figure 6. Si 2p X-ray photoelectron spectrum of SiO_2/Si substrate (this work)

For gold as shown in Figure 7, the most commonly analyzed XPS feature is the 4f-levels near 85 eV. The triplet peak observed is the result of convolution of four peaks; corresponding to two spin-orbit doublets of Au^{3+} and Au.

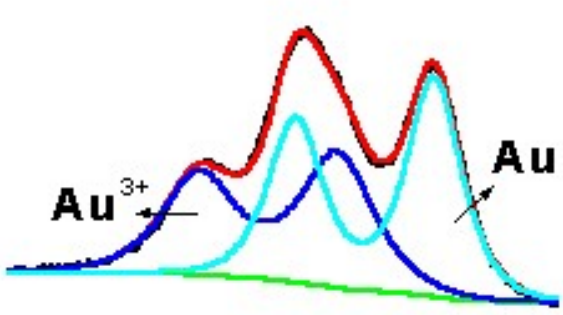

Figure 7. Representation of the combination of Au^{3+} and Au^{0} peaks (this work)

4f binding energy of gold in several oxidation states or gold cluster compounds with different oxidation states have been reported to range from 84 to 87.6 eV, as given in Table 4 [16,17].

Table 4. Binding energy value for different gold compounds [16,17]

Compound	Binding Energy (eV)
Au	84
$(PPh_3)AuCl$	85.2
$(PPh_3)AuI$	85.4
$(PPh_3)AuCl_3$	87.5
$(PPh_3)AuI_3$	87.6

1.3.1.2 Local Environment Dependent Chemical Shift

X-Ray photoelectron spectra can also provide information about an element's chemical environment. The chemical environment of an atom affects the strength with which electrons are bound to it. Atoms associated with different chemical environments produce peaks with slightly different binding energies, which is also referred to as chemical shift. Table 5 gives binding energy values for different sodium compounds. Binding energy change with the change of anion type shows the effect of chemical environment explicitly.

Table 5. Binding energy values for sodium compounds [23]

Compound	Binding energy (eV)
NaF	1071.2
$NaBF_4$	1072.7
NaBr	1071.7
NaH_2PO_4	1072.0
NaCl	1071.6

1.3.2 Final State Effects

When photoelectron is ejected from the atom, there will occur a hole in the core level resulting in positive charge. Other energy levels of the emitted atom (intra-atomic) and energy levels of neighbor atoms (extra-atomic) interact with this hole so as to stabilize this positive charge resulting in a decrease in the energy of the atomic levels called relaxation energy as illustrated in Figure 8. These factors serving to stabilize the positively charged core-hole state are called final state effects. Particle-size and environmental effects are types of final state effects [21].

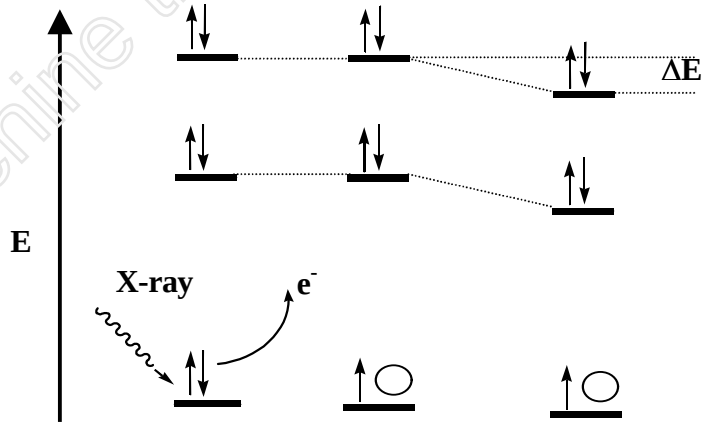

Figure 8. Illustration for the stabilization of energy levels during photoemission process (Final state effect)

1.3.2.1 Final State Effect due to Local Environmental

Due to environment of the analyzed atom, Na(I) compounds are compared while explaining the environment dependent shift as an initial state effect. When binding energy of sodium and sodium chloride are considered, we realize a reverse relationship between the chemical shift and the oxidation state. Although it is expected that binding energy of sodium atom in NaCl should be larger than that of sodium metal, one observes that binding energy values of the two species are not different from each other. This is the result of response of conduction electrons to the hole created after photoemission due to screening [39]. Na metal having a higher density of electrons at the Fermi level responds to created hole much easier than those in ionic compounds.

Table 6. Binding energy values for sodium and sodium chloride

Compound	Binding energy (eV)
Na	1071.8
NaCl	1071.6
NaBr	1071.7
NaF	1071.2

1.3.2.2 Particle-size Effect

It was established long ago that the particle size also affects the measured binding energy. For example; Youngquist et al. prepared gold clusters on carbon with different thicknesses to investigate the effect of physical environment on the binding energy [40]. Figure 9 shows the dependence of binding energy on the gold coverage (atoms/cm^2). Binding energy of gold cluster changes by about 0.6 eV as the gold thickness increases from 0.1 ML to 10 ML. It is known that 1 monolayer (ML) which refers to the average coverage of gold particles on the substrate surface is equal to approximately 1.5 *10^{15} atoms.cm^{-2}. As the gold coverage decreases, binding energy shifts to more positive values due to final-state effect. When the electrons are emitted from the sample, it will be more difficult to stabilize the system as the gold coverage decreases. It is also noteworthy to say that when gold cluster reaches to 1ML, binding energy of gold is about 0.3 eV higher than that of bulk gold.

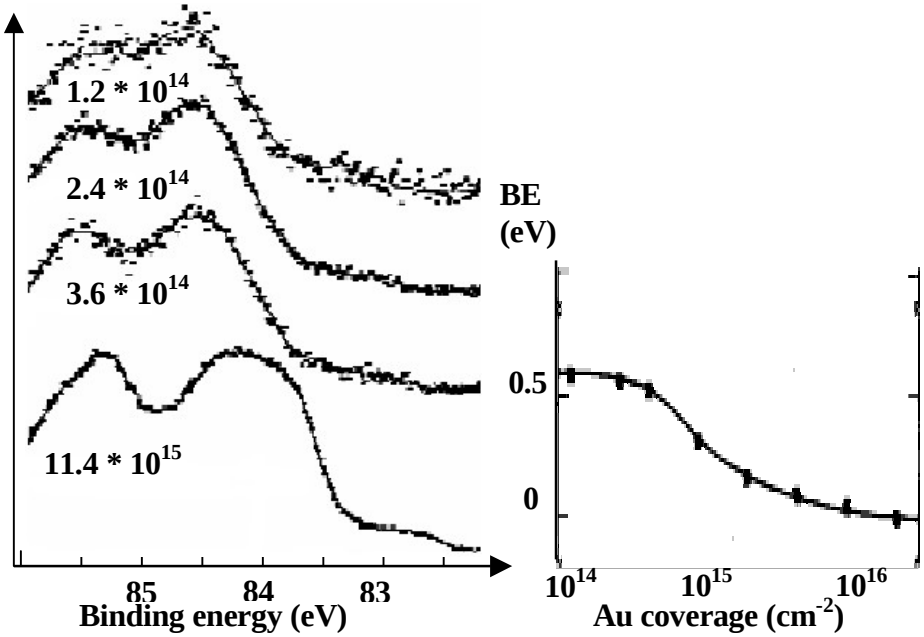

Figure 9. Particle size dependence of binding energy of gold [40]

1.3.3 Charging Effect

As the electrons are emitted from the sample, a positive charge develops on the substrate as shown in the Figure 10. If the sample is conducting, the positive charge due to the ejected photoelectron is replenished instantaneously with an electron that is withdrawn from the spectrometer ground. However, if the conductivity is not high, a positive voltage starts to develop on the surface with respect to the spectrometer ground resulting in a decrease in the atomic energy levels of the substrate as shown in Figure 11. When charging is present, binding energy will then be equal to:

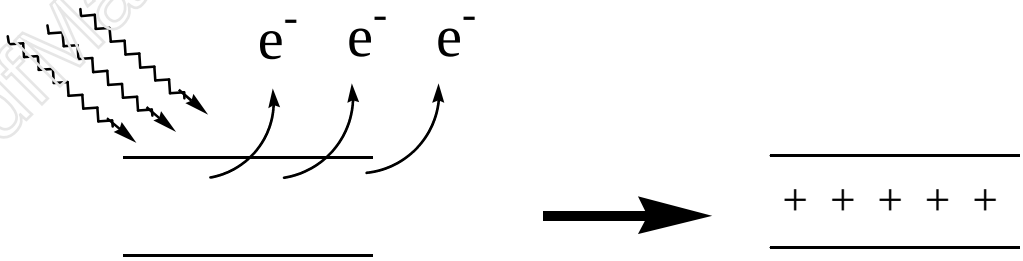

Figure 10. Schematic illustration of charging during photoemission

$$E_B = h\nu - E_K - \varphi_S + C \text{ [41]} \quad (8)$$

where φ_S is the spectrometer work function and C is the change in the atomic energy levels due to charging. It will be more difficult to emit an electron as the positive voltage increases on the sample resulting in an increase in the measured chemical shift.

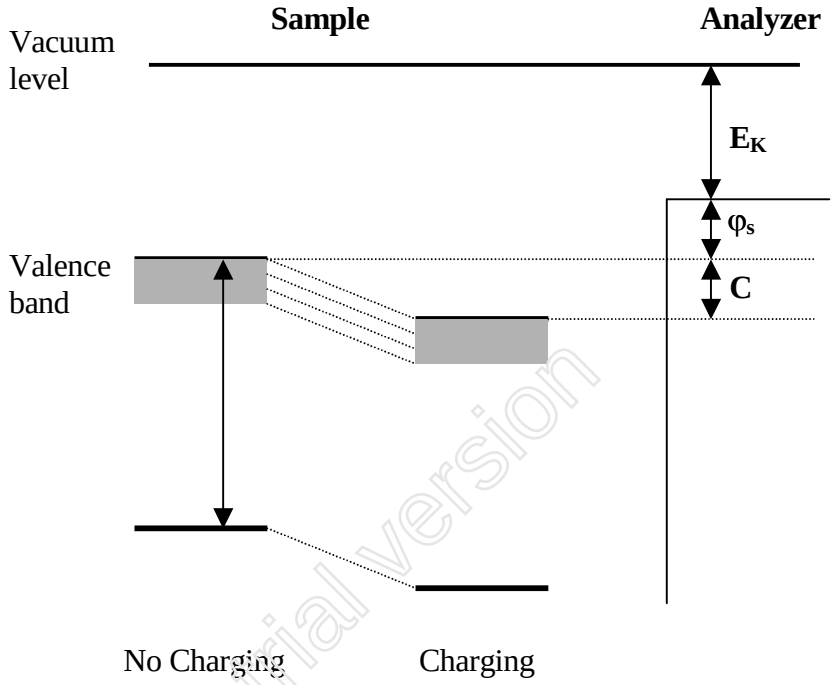

Figure 11. Change in atomic energy levels when charging is present

Contribution of C parameter to the measured chemical shift could be different for substrates consisting of more than one layer according to the conducting behavior of the cluster and the cluster-substrate interaction. This difference could also appear between the same atoms of the substrate due to the morphological variations in the system [41]. This is called *differential charging.*

Although φ_S value in Equation 8 is determined by the calibration of the instrument, determination of the contribution of charging (C) to the measured binding energy is not easy. Determination of C-value has been one of the aims for scientists dealing with

surface science for many years [42-49]. Chemical shift that is the result of charging effect could be avoided by exposing surface to neutralizing flux of low energy electrons 'flood gun' or selection of a suitable reference point to eliminate the contribution of charging to the measured chemical shift [21]. In addition to these, external bias method can be applied to investigate the occurrence and the contribution of charging to measured chemical shift.

1.4 Application of an External Bias

In order to understand the charging behavior of samples, numerous efforts have been performed using different techniques. One of the applicable methods to investigate the effect of charging on the measured chemical shift is applying an external bias to the sample with the set-up shown in Figure 12.a) [11]. When this method is applied to SiO_2/Si substrate, one can obtain XPS spectrum of SiO_2/Si sample without and with +10V and -10V as shown in Figure 12.b).

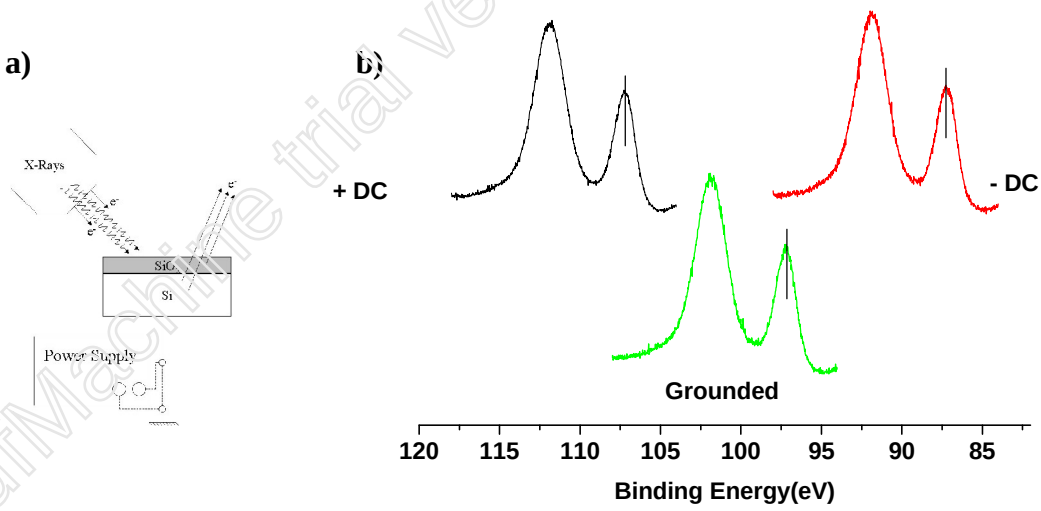

Figure 12. a) Schematic diagram of the XPS setup with external bias **b)** XPS of SiO_2/Si system without and with +10V and -10V

Although a shift is observed that is equal to the applied external bias, the measured binding energy difference between Si^{4+} and Si^{0} is larger when negative bias is applied and is smaller when positive voltage is applied as shown in Figure 13. Binding energy difference of Si^{4+} 2p peak is about 0.3 eV going from –10V to +10V which is significant.

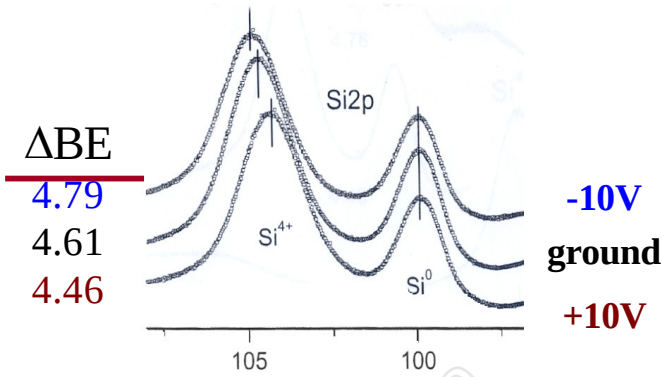

Figure 13. XPS spectrum of SiO_2/Si system without and with +10V and –10V when peaks are correlated according to Si^{0} 2p peak [11]

During the course of X-ray exposure of the sample, secondary electrons are also created. Emission of the secondary electrons from the sample is also influenced by application of an external bias. When stray electrons are also considered, there are different sources of electrons falling onto or emitted from the sample. Stray electrons and formation of secondary electrons are illustrated in Figure 14. In addition, another electron source (a filament) can also be introduced to increase the number of stray electrons falling onto the sample. These electrons can also contribute to charge neutralization. When positive external bias is applied, these electrons will be attracted by the substrate surface for neutralization which causes binding energy difference between Si^{4+} and Si^{0} 2p peak to decrease. The same behavior will lead to increase in the binding energy difference when negative bias is applied.

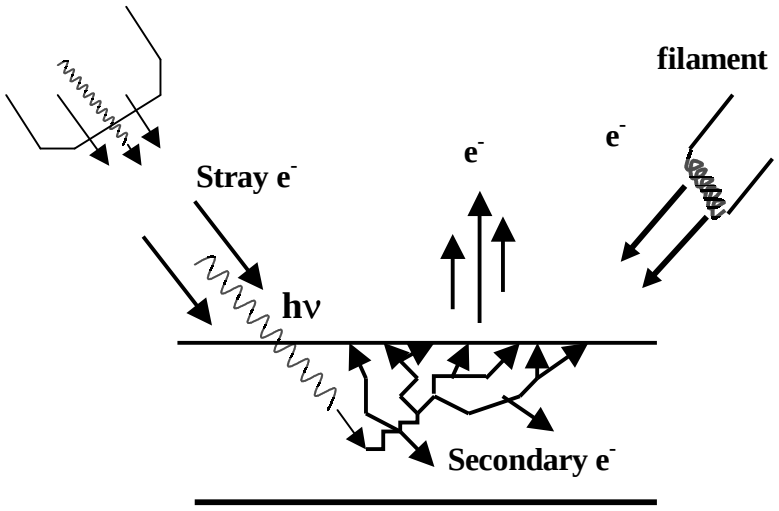

Figure 14. Illustration of the formation of stray and secondary electrons

Auger parameters can be also determined to investigate the contribution of charging to the measured binding energy difference.

1.5 Auger Parameter

During photoemission process, in addition to the formation of photoelectrons, Auger electrons are produced where one electron drops down to fill the hole and another electron is ejected during the filling of the hole The difference in the formation of photoelectrons and Auger electrons are shown in Figure 15.

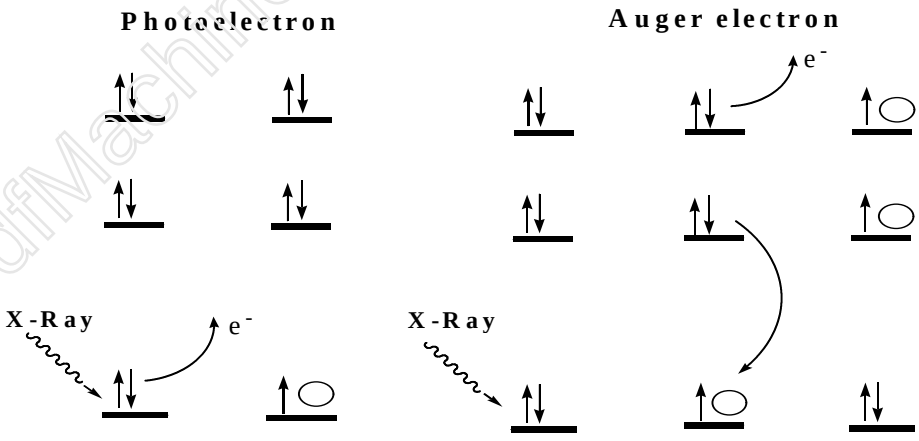

Figure 15. Production of photoelectron and Auger electron

The concept of Auger parameter was evaluated when it was observed that chemical shifts of photoelectrons and Auger electrons are different. Since there occurs a shift in both peaks, the difference between their kinetic energies gives a characteristic property for each system. By definition Auger parameter should be equal to $\alpha + h\nu$ where α is equal to the difference between Si 2p and Si KLL lines in Figure 16. It was demonstrated that the Auger Parameter is much more sensitive to chemical and physical differences [39, 50-52].

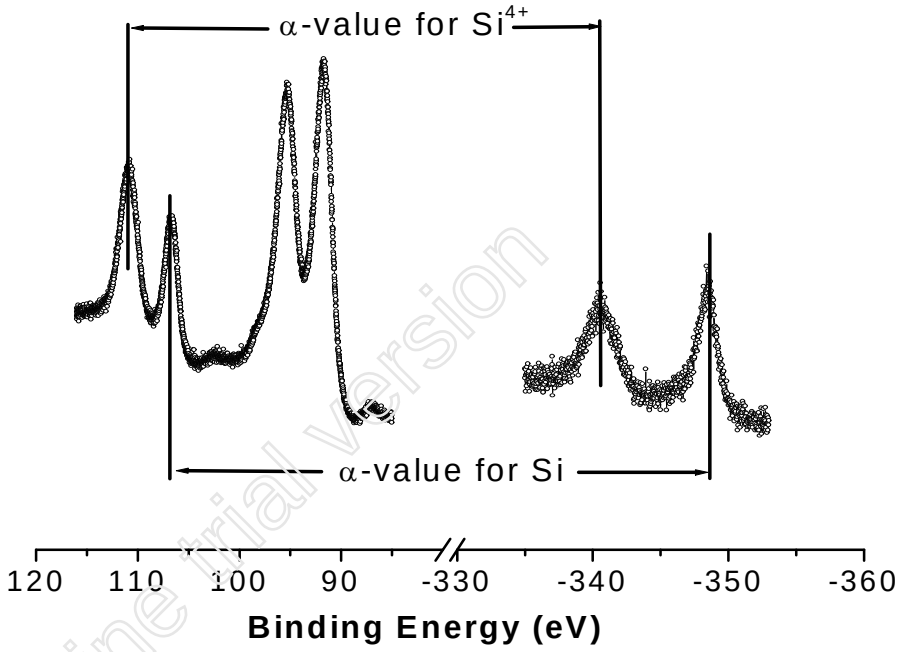

Figure 16. Measurement of α-value for Si^{4+} and Si

1.8 Properties of SiO_2/Si System as Determined by XPS

Extensive effort has been devoted to the XPS properties of SiO_2/Si substrate in order to investigate electronic properties of the substrate and to understand the composition of SiO_2/Si system. Studies, aiming this, have shown that binding energy difference increases from 3.2 to 5.0 eV as the SiO_2 thickness increases as shown in Figure 17 [2-5,7,8,11]. Although the exact reason for this behavior is not known explicitly, chemical shift is thought to be the result of extra atomic relaxation energy –final state effect-or charging

effect or the combination of the two factors. Ishizaka and Iwata have proposed that this chemical shift is solely due to differential charging and the exact binding energy difference between Si^{4+} and Si^{0} 2p peaks is 3.0 ± 0.2 eV [5]. However, Zhang et al. stated that the shift of the Si^{4+} 2p peak is due to the change in the extra atomic relaxation energy as the oxide thickness changes from 0.6 to 3 nm. They claimed that they avoided initial state effects and measured only the final state effects by preparing $Si_8H_8O_{12}$ clusters on the

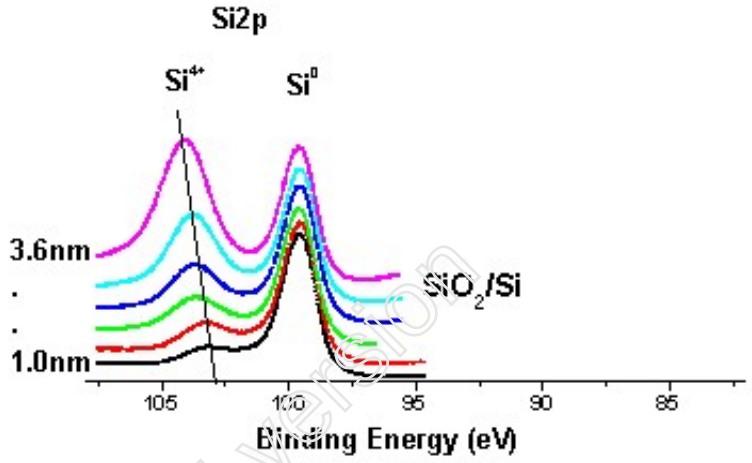

Figure 17. Increase in the binding energy of Si^{4+} 2p peak with the increase in SiO_2 thickness when Si 2p peak is chosen as the reference

Si(100) surface [3,4]. They also reported that when the oxide thickness gets thicker than 3 nm, differential charging effect occurs, and the shift for oxide thicker than 3 nm is the result of differential charging. Kobayashi et al. who covered the top of silicon oxide layer by Pd overlayer (~ 3 nm) in order to prevent most of the differential charging on the SiO_2 layer, also put this claim forward [8]. Recently, Süzer and Ulgut observed that differential charging is present in the SiO_2/Si system down to a thickness of 1 nm by applying external bias method to SiO_2/Si substrate [11]. Figure 18 explains the results of their study briefly. The differential charging is measured when oxide thickness is about 1 nm and contribution of charging increases as the oxide thickness increases.

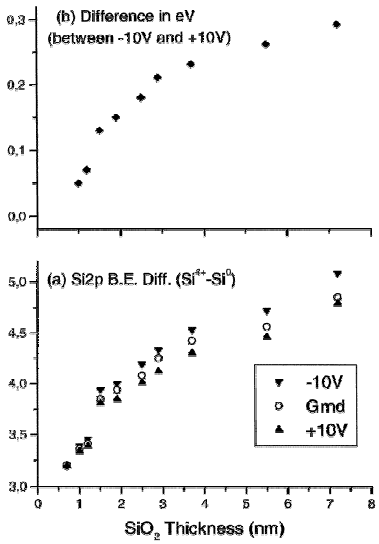

Figure 18. a) Variation of the Si 2p binding energy difference between the oxide and substrate with the thickness of the oxide layer recorded without and with application of +10 and –10V bias, **b)** Variation of the binding energy difference between the sample subjected to –10 and +10V bias with the thickness of the oxide layer.

1.7 Preparation of Gold Particles:

Considering the factors that influence measured binding energy and methods to separate these factors listed above, chemical shift of gold particles on SiO_2/Si substrate will be investigated to gain information about the interaction between SiO_2 and gold particles. Since it is observed that properties of metal particles change considerably with the change in their particle size, gold atoms with different sizes, and preparation methods are employed.

1.7.1 Deposition of Gold Particles from Aqueous Solution

Besides general deposition techniques such as electrochemical [53,54], chemical (electroless) [55] and physical vapor deposition methods [56-60], gold can also be deposited from $AuCl_4^-$ aqueous solution on SiO_2/Si substrate [61-63] with subsequent *reduction* by X-ray and *nucleation* of gold particles.

1.7.1.1 Reduction Process

As explained previously, electrons from the analyzed sample are emitted during photoemission process. As the emission progresses, the electrons created (mostly secondary electrons) may also induce reduction of the atom analyzed. The effect of active sites of silicon surface on the reduction was also emphasized in addition to secondary electrons created [64]. It was reported that reduction process is valid for metals that have

positive reduction potentials such as Au^{3+}(+1.5 V) and Hg^{2+} (+0.9 V) while no reduction was observed for metals having negative or small reduction potentials, indicating that a straight correlation could be established between electrochemical reduction potentials and the reduction by X-rays.

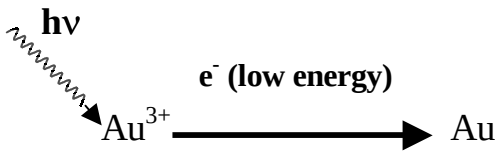

Figure 19. Reduction of Au^{3+} during photoemission process

1.7.1.2 Nucleation and Growth

Reduction process during photoemission will result in the formation of Au^{o} particles within the Au^{3+} salt on the substrate. Since the structure of the reduced gold particles affects the measured binding energy of Au particles, investigation of the structure of gold particles and possible mechanisms of the reduction process should be the first aim. Possible reduction mechanisms are shown in Figure 20.

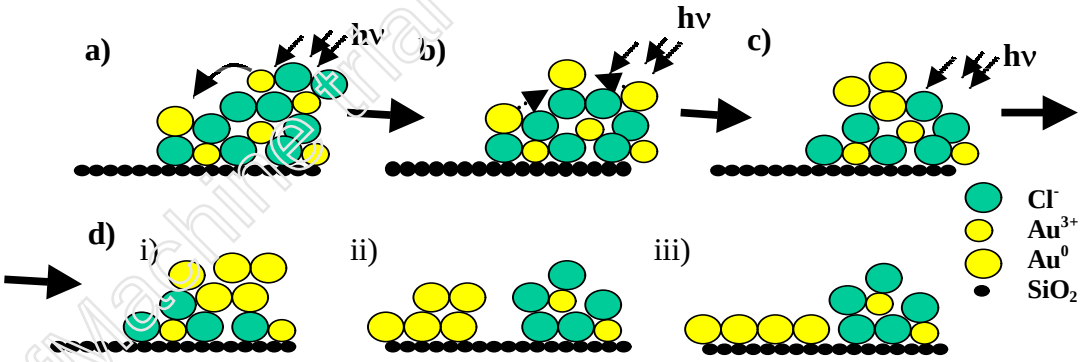

Figure 20. Possible reaction mechanisms for the reduction of gold on SiO_2 substrate, **a)** before X-ray exposure, **b)** movement of reduced gold atoms from Au^{3+} atoms, **c)** nucleation process, **d)** i) growth of reduced gold particles via forming island-like structures (3D-growth) among within Au^{3+} salt, ii) growth of reduced gold particles via forming island-like structures (3D-growth) -further to Au^{3+} salt-, iii) growth of reduced gold particles on the substrate two-dimensionally (2D-growth)

Following the X-ray exposure, reduction process continues with the movement of reduced gold particles to combine with each other. This process is called nucleation, which is briefly the tendency of populations to cluster in settlements of increasing size and density, and is the necessary step for the growth of particles. During nucleation process, reduced gold atoms with the combining of a few gold atoms to form a more stable nanostructure. When the amount of reduced gold particles increase on the surface and more than a few gold atoms begin to combine, growth process begins. Considering that gold has one of the largest cohesive energies (3.81 eV/atom [65]) among metals, three possible growth mechanisms are suggested for gold clusters as shown in Figure 20. First mechanism is the three-dimensional growth where gold particles form island-like structures within Au^{3+} salt. Second mechanism differs in that gold particles form island-like structures after they leave from Au^{3+} salt. Final possible mechanism is quasi-two-dimensional (2D) growth of gold particles on the SiO_2 surface via covering the substrate surface smoothly. Goodman et al. reported that gold particles deposited on silica surface with physical vapor deposition method grow two-dimensionally after the coverage reaches 0.1 ML (monolayers) whereas particles prefers to grow three-dimensionally until the coverage reaches 0.1 ML (1 ML $\approx 1.5*10^{15}$ atoms.cm^{-2}). Noting that monolayer is related to the atomic density of gold particles (cm^{-2}), gold prefers to grow two-dimensionally when 10% of the substrate surface is covered with gold particles. Part of this thesis is devoted to enlighten the mechanism of this process.

1.7.2 Capped Gold Particles

Since metal nanoparticles have received great attention due their importance in future MOS-design, numerous investigations have been performed on capped gold particles since the effect of citrate ions on the preparation of gold nanoparticles had been understood [66-68]. Turkevich et al. observed a wine red colour when they heat a solution containing tetrachloroaurate(III), $AuCl_4^-$, and trisodiumcitrate to 60-80^oC [66]. By means of citrate reagent, the size of gold particles can be controlled and capped gold particles having a mean radius of 8 - 10 nm could be prepared as shown in Figure 21 [69]. Citrate ions serve as both reducing and capping agents during the procedure.

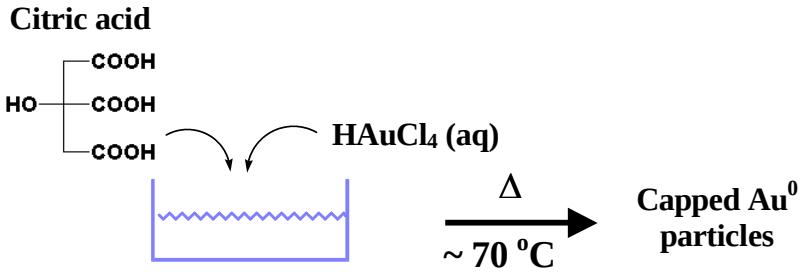

Figure 21. Preparation of citrate capped gold particles

Properties of citrate capped gold particles could be listed as follows:

- When one considers a citrate capped nanoparticle having a diameter of 10 nm, the number of gold atoms can be estimated as $5*10^4$ per one nanoparticle.

- Besides their easy preparation as shown in Figure 21, a sharp absorption peak of citrate capped gold nanoparticles at 523 nm due to the oscillations of electrons in the valance band is used for the characterization of these nanoparticles as shown in Figure 22 [68-72].

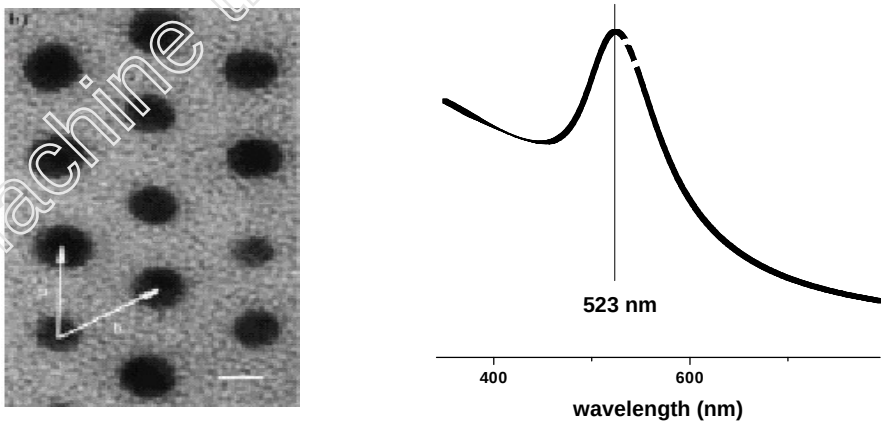

Figure 22. a) TEM image [69] (scale bar is 7 nm) and **b)** Vis-absorption spectrum of citrate capped gold nanoparticles (this work)

- Another characteristics of citrate capped gold particles is the shift of absorption bands to wavelengths higher than 523 nm with the increase in particle size (Figure 23) [68,70].

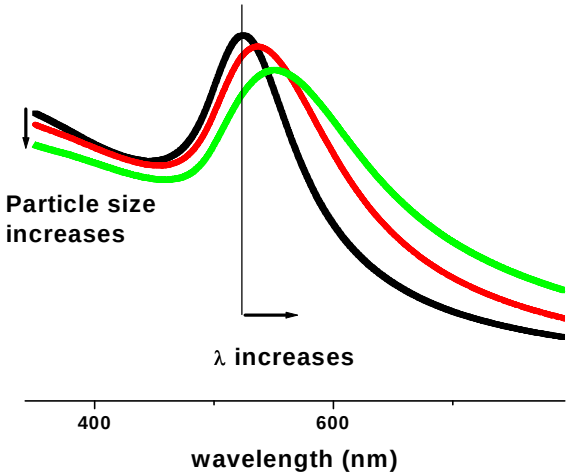

Figure 23. Change of absorption wavelength with cluster size (this work)

In addition to the Vis-absorption method, estimation of particle size could also be obtained by electrophoretic methods. In electrophoresis, charged particles travel different path in the gel with the applied voltage. Speeds of the particles vary according to their charges, sizes and certain properties of the gel. The smaller the size of the species has and the greater the charge it has, the faster it runs in the gel. Electrophoresis apparatus is shown in Figure 24.

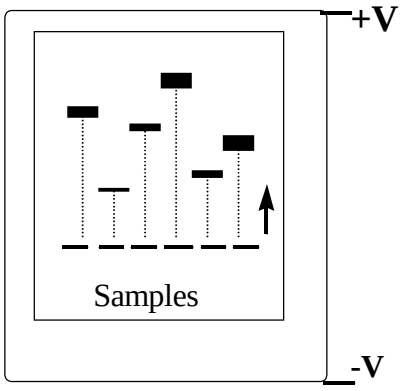

Figure 24. A simple schematic of electrophoresis method

- It is also known that citrate agent that covers the gold particles could be replaced by many anions which have oxygen, nitrogen or sulfur consisting functional groups such as sulfate, phosphate, carbonate and tannic acid without changing the Vis-characteristics of gold nanoparticles. This behavior of gold particles allows them to be used in specific reactions, which are selective to the molecule that serves as a capping agent [68,71].

- Absorption peak of gold particles in different solvents could shift to higher/lower wavelengths according to the dielectric constant of the solvent [68,72].

- When capped gold particles are deposited on silicon surface, gold particles combine with each other without increasing the particle size [73,74]. This process is called aggregation where the difference between aggregation and growth are illustrated in Figure 25.

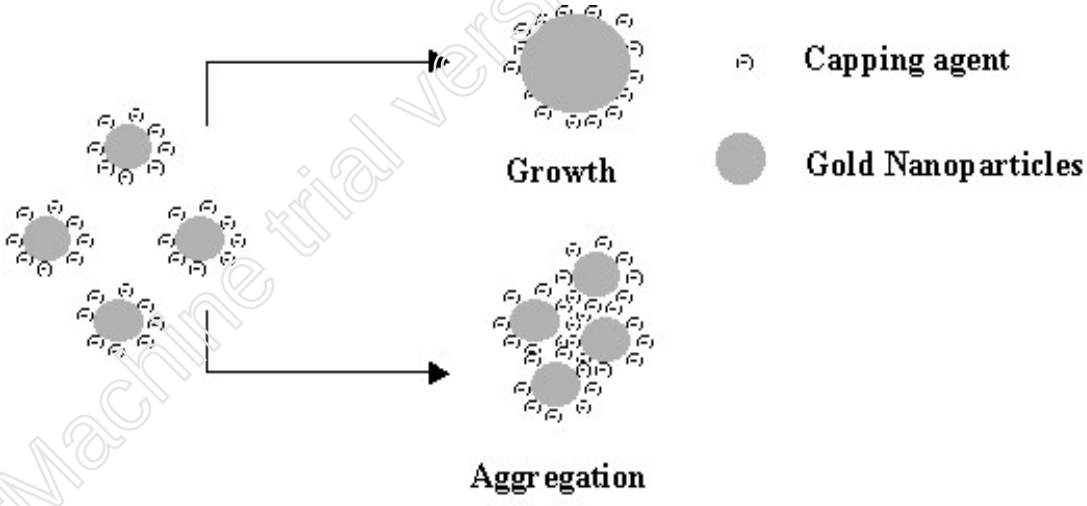

Figure 25. Growth and aggregation of capped gold nanoparticles

As also illustrated in Figure 25, citrate capped gold nanoparticles have minus charge surrounding the nanoparticle due to the citrate anion [75,76]. Therefore, it should be pointed out that citrate capped gold particles may also contribute to the chemical shift not only by changing the particle size but also due to their charging capacity. The effect of

particle size and the type of the capping agent on the measured binding energy will be discussed in this thesis.

1.7.3 Chemically Reduced Gold Particles

Due to its positive reduction potential, Au(III) could also be reduced to its metallic state by the means of mild reducing agents such as $NaBH_4$ [71]. Since particle size is not controlled by any factor, larger gold particles are prepared compared to capped gold nanoparticles.

2. AIM OF THE PRESENT WORK

The reasons for the measured chemical shift of gold particles on the SiO_2/Si substrate will be discussed in order to investigate the nature of the interaction -physical or chemical- between gold and silicon dioxide substrate. Gold particles in different matrices and with different particle sizes have been prepared and investigated for this purpose.

Although there could be many factors contributing to the measured chemical shift, some factors such as charging, could be avoided when suitable methods are applied. When a suitable reference point is chosen, which has similar charging behavior to that of gold, charging effect could be subtracted from measured chemical shift of gold. One of the purposes of the present thesis is to designate the reference point when gold particles are considered. In addition to choosing a reference point, application of external bias technique and Auger Parameter method will also be used to investigate the contribution of charging to the measured chemical shifts.

3. EXPERIMENTAL

3.1 Reagents

p-doped Si (100) wafers were used throughout this work. $HAuCl_4.H_2O$, sodium citrate, tannic acid, sodium sulfate, $NaBH_4$, glycerol purchased from Aldrich, agarose from Prona, TAE (tris, acetic acid, EDTA mixture) buffer from Cole-Parmer were used.

3.2 Procedure

3.2.1 Preparation of SiO_2/Si System

Si (100) substrate was allowed to stay in concentrated HF solution for 45-60 seconds to remove native oxide layer and rinsed with deionized water and dried. Clean Si (100) samples were heated in air at 500^0C using furnace. Duration of heating was varied from 1 to 4 hours to have SiO_2/Si systems with different oxide thicknesses (~3 to 9 nm).

3.2.2 Preparation of Au ($AuCl_4^-$)/SiO_2/Si System

After SiO_2/Si system was prepared thermally, either the substrate was allowed to stay in solution containing ~0.034 % (w/v) of tetrachloroauric acid for various durations or tetrachloroauric acid of the same concentration was dropped on the substrate and kept in air at room temperature until water is evaporated.

3.2.3 Preparation of Au (capped)/SiO_2/Si System

120 mL of 0.008 % (w/v) solution of tetrachloroauric acid were heated to 70^0C. Then, 1 mL of 7.6 % (w/v) solution of sodium citrate was added to the gold solution (pH ≈ 4.5). The mixture was stirred at 70^0C for 3 hours followed by cooling. Solution turned to a color of wine red indicating the formation of citrate capped gold particles. In addition, absorption band at 523 nm observed by UV-vis absorption spectroscopy indicated the formation of capped gold particles.

To prepare tannic acid- citrate capped gold particles, 2 mL of 1 % (w/v) solution of tannic acid were added together with 1 mL of 7.6 % (w/v) solution of sodium citrate to the gold solution at the beginning. The same procedure was applied as in the previous

section and tannic acid-citrate capped gold particles were prepared which have similar optical properties.

Finally, gold particles whose surfaces were passivated with sulfate anions were also prepared. In order to isolate gold particles from excess citrate and tannic acid buffer, 1 g of sodium sulfate was added to a solution of 20 mL of tannic acid-citrate capped gold particles. Solution was centrifuged and liquid part was discarded. Collected gold particles were washed with minimal amount of distilled water and centrifuged again. Liquid part was discarded again and precipitate was redissolved in water for optical characterization [68].

The same procedure, which was applied in previous sections, was used to deposit capped gold nanoparticles on SiO_2/Si substrate.

3.2.4 Preparation of Au (reduced with $NaBH_4$)/SiO_2/Si System

0.1 g of $NaBH_4$ was added to 10 mL of tetrachloroauric acid solution of 0.034 % (w/v) to reduce gold to its metallic state. Chemically reduced gold particles were deposited on SiO_2/Si substrate as explained in previous sections.

3.3 Instrumentation

3.3.1 XPS Studies

KRATOS ES300 spectrometer with a Mg K_α (not monochromatized) source at 1253.6 eV was used to record XPS spectra. The base pressure was kept below 10^{-8} torr throughout the measurements. XPS peaks were fitted using XPSPEAK 4.0 fitting program. An angle of 90^o was used as take-off angle.

3.3.2 Vis-absorption Studies

Vis-absorption spectra were recorded using the double beam Varian Cary 5 spectrophotometer with a scan rate of 90 nm/min over the wavelength range from 1400 nm to 350 nm.

In order to have Vis-absorption spectra of capped gold particles, they were measured directly by using a plastic cuvette. Then, solutions of capped gold particles were dropped on glass/quartz and dried in air at room temperature to form uniform films. After Vis-absorption spectra of these films were taken, films were inserted in minimal amount of deionized water to dissolve capped gold particles on the substrate. Substrates were removed from the solution and Vis-absorption spectra of solutions were taken again to observe whether there has occurred any shift in the absorption peak.

3.3.3 Electrophoresis Studies

10 μL of glycerol was added to 30 μL of solution containing capped gold particles (3:1 volume ratio) to prevent the solution to disperse in TAE buffer during electrophoresis. 150 ml of solution containing 1 g of agarose was prepared. The resulting solution was boiled until the milky color disappeared and cooled. Then, agarose solution was poured on the gel bed, which was taped from both ends. This was followed by placing the gel comb instantly into the desired slot. Solution was allowed to cool until it turns opaque. Gel tapes were removed from each end and comb was removed gently. Tray was placed in the compartment. Enough TAE buffer was added to fill both reservoirs and overflow the surface of the gel to a depth of 2-3 mm. After samples were loaded into the sample wells, voltage was applied to both ends of the unit (100V) as shown in Figure 26.

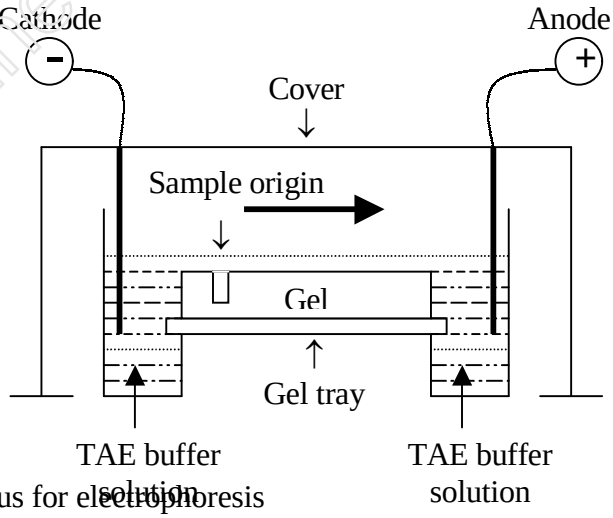

Figure 26. Apparatus for electrophoresis

4. RESULTS & DISCUSSIONS

4.1 Choosing the Reference Point

As in all spectroscopic techniques, a reference point is also required to determine the binding energies in XPS technique. In order to choose a reference point for gold particles on SiO_2/Si system, firstly, charging characteristics of Au($AuCl_4^-$)/SiO_2/Si system must be investigated. To separate the chemical shift due to the charging of gold clusters and to determine the binding energy of gold cluster more accurately, a reference point should be chosen, which shows similar charging to that of the gold layer. Spectra of two Au($AuCl_4^-$)/ SiO_2/Si systems with different thicknesses of SiO_2 layer that are equal to 5.3 nm and 1.2 nm are shown in Figure 27. It is clearly seen that gold layer shifts in the same direction of the Si^{4+} peak, indicating a similarity in the charging characteristics of SiO_2 and gold layer. So Si^{4+} peak could be used as the reference peak while studying gold clusters.

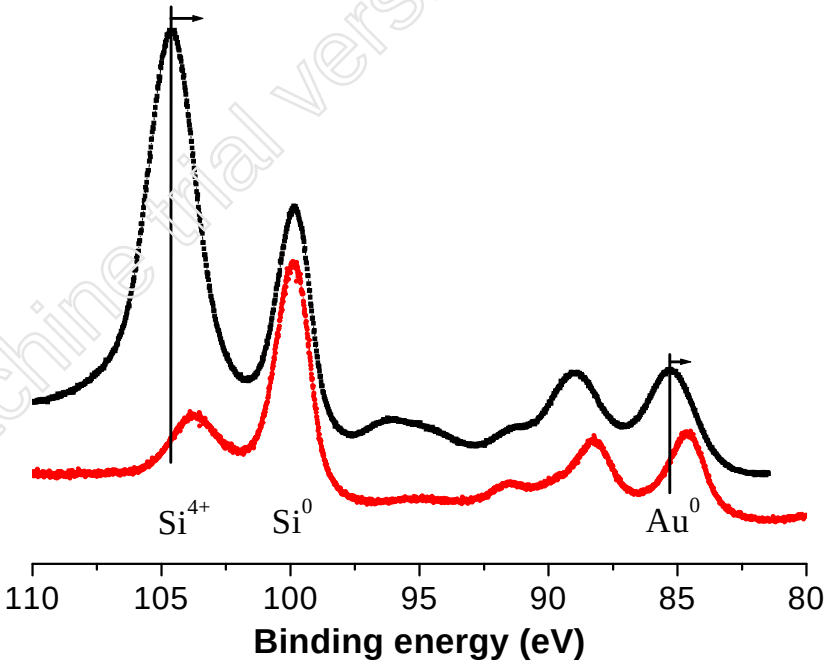

Figure 27. XPS Spectra of Au($AuCl_4^-$)/SiO_2/Si systems with different SiO_2 thicknesses

Similar shifts have also been observed when external bias is applied to the substrate as shown in Figure 28. Binding energy difference between Si^{4+} and Au^0 does not change significantly despite the change in binding energy difference between Si^{4+} and Si^0 as tabulated in Table 7 reinforcing our conclusion that SiO_2 layer could be used as the reference peak while studying gold clusters.

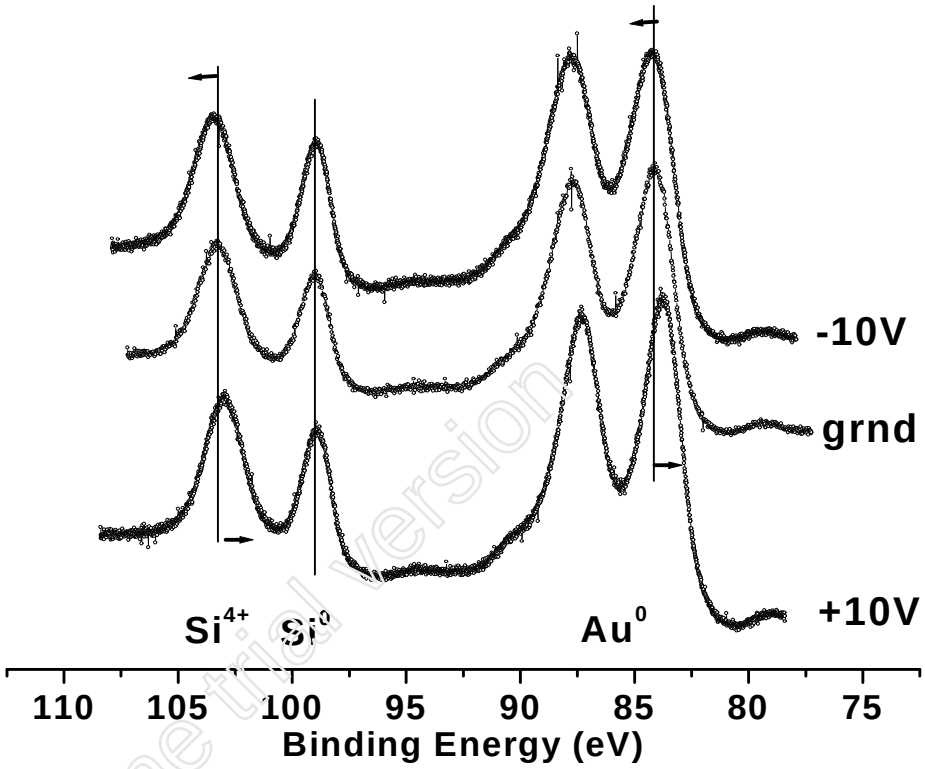

Figure 28. XPS Spectra of Au(citrate)/SiO_2/Si system without and with +10V and –10V external bias

Table 7. Measured binding energy values of the sample containing citrate capped gold particles on SiO_2/Si

	ΔBE (Si^{4+} - Si^0) (eV)	**ΔBE (Si^{4+} - Au^0) (eV)**
+10 V	3.92	19.11
Grnd	4.28	19.16
-10 V	4.47	19.13

The second problem is to select a reference point for the reference peak (i.e. Si^{4+}). For this purpose, gold is deposited on SiO_2/Si system using physical vapor deposition method. Using this method, a gold layer having a definite thickness of uniform gold layer could be grown on SiO_2/Si system. Three different samples with gold coverages of 0.5, 3, 5 nm were prepared. Since no significant binding energy difference between Si^{4+} and Au^0 was observed among these samples, it is assumed that all of the samples behave like bulk gold. Noting the fact that XPS is a surface sensitive technique within a thickness of less than 20 nm, this assumption is valid. Accordingly, the binding energy difference between Au 4f and Si^{4+} 2p can be taken as 19.43 eV when sample having a gold coverage of 3 nm is used as shown in Figure 29. When the binding energy of Au 4f peak is taken as 84.00 eV which is the value for bulk gold, the binding energy for Si^{4+} 2p peak becomes 103.43 eV which will be used as our reference point.

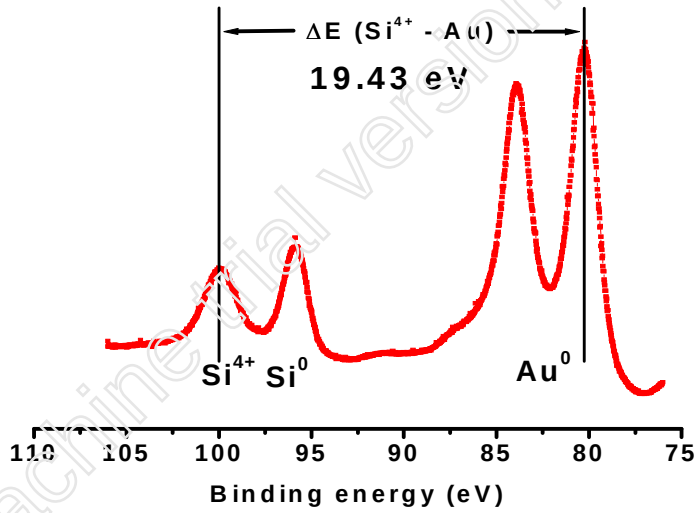

Figure 29. Measurement of reference binding energy for Si^{4+}

It should be also noted that discussion for a suitable reference point will be continued throughout the thesis to establish if the SiO_2 layer is the right choice. Although direct interaction of SiO_2 layer with gold particles supports this assumption, experiments about gold particles with different cluster size and in different matrices will lead us to make a more convincing conclusion.

4.2 Gold particles on SiO_2/Si Substrate Deposited from Solution

4.2.1 X-ray Induced Reduction of Au^{3+}

As explained in the introduction part, certain metal ions with large positive reduction potentials are easily reduced during the exposure to X-Rays [63,64]. As also shown in Figure 30, Au^{3+} is reduced to its metallic state during X-ray exposure. Increase in the Au^0 peak at the expense of Au^{3+} peak with time indicates explicitly the reduction.

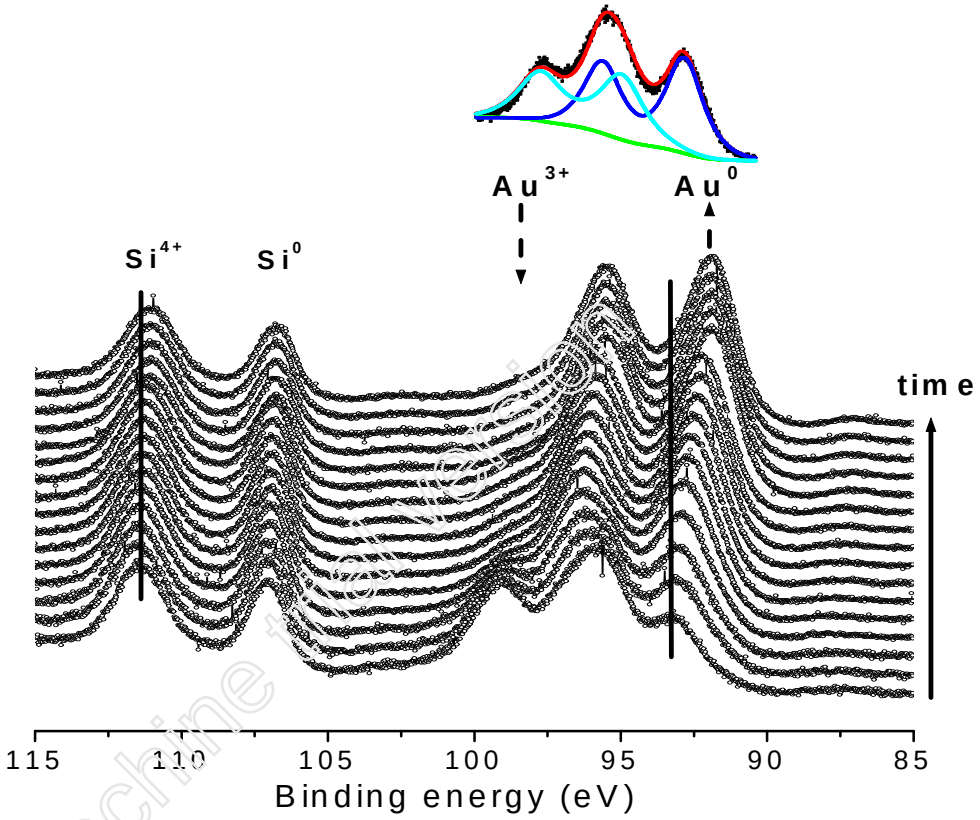

Figure 30. Reduction of Au^{3+} during X-ray Exposure

In order to compare the concentrations of Au^{3+} and Au^0 atoms on the substrate surface explicitly, Au^{3+} and Au^0 peak areas ratioed against Si^{4+} peak area with time and the measured binding energy difference are plotted in Figure 31. Both plots have exponential behavior indicating that most of the reduction process occurred in

approximately in the first three hours of the X-ray exposure and the rate of reduction process decreases as concentration of the Au^{3+} atoms decreases.

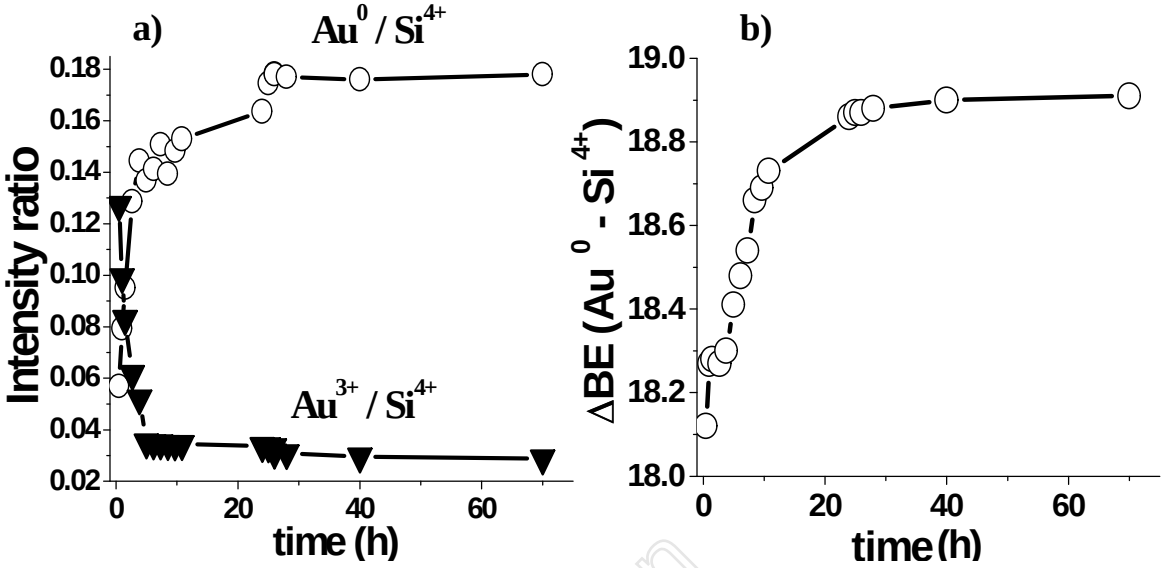

Figure 31. a) Atomic ratios of Au^{3+} and Au^{0} peaks to Si^{4+} peak vs time (intensity ratios were calculated by dividing the peak ratios with the photo-ionization cross-sections, $\sigma(Au\ 4f_{7/2} + Au\ 4f_{5/2}) = 17.47$, $\sigma(Si\ 2p_{3/2} + Si\ 2p_{1/2}) = 0.865$) **b)** Binding energy difference between Au^{0} and Si^{4+} peaks vs time

In addition to the X-ray induced reduction of Au^{3+}, a shift in the binding energy of Au^{0} is also observed. It is well-known that binding energy of gold decreases to that of bulk gold as the particle size of the gold cluster increases and approaches to bulk gold [40, 60, 77]. As shown in Figure 31.b), the binding energy difference between Au^{0} and Si^{4+} peaks increases from 18.12 eV to 18.91 eV, hence the binding energy of gold decreases about 0.79 eV indicating possibly a nucleation and growth process. Exponential behavior shows that the rate of nucleation process decreases with time similar to rate of reduction process. Resemblance of both plots in Figure 31 gives strong evidence that reduction and nucleation processes occur together. Shift in binding energy of gold can be seen more explicitly in Figure 32 where only the initial and final spectra are shown.

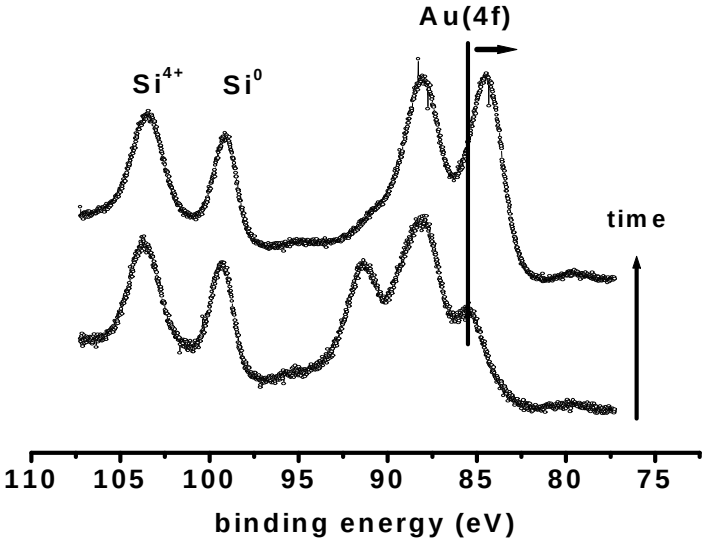

Figure 32. Initial (after 0.5 hour) and final (after 16 hours) X-ray photoelectron spectra of gold sample deposited from aqueous solution (with X-ray power= 50 W)

When Si^{4+} 2p peak (103.43 eV) is taken as reference, BE of Au^0 is calculated as going from 85.31 to 84.52 eV. Goodman et al. reported a similar study where binding energy of gold with different gold coverages are measured and plotted as shown in Figure 33 [60]. Although Au^0 particles were prepared with physical vapor deposition method in their study, gold clusters deposited from solution gave similar results in our study. According to Figure 33, binding energy of gold cluster changes about 1.8 eV as the gold coverage increases from 0.1 ML to 25 ML. Using the plot depicted by Goodman, average

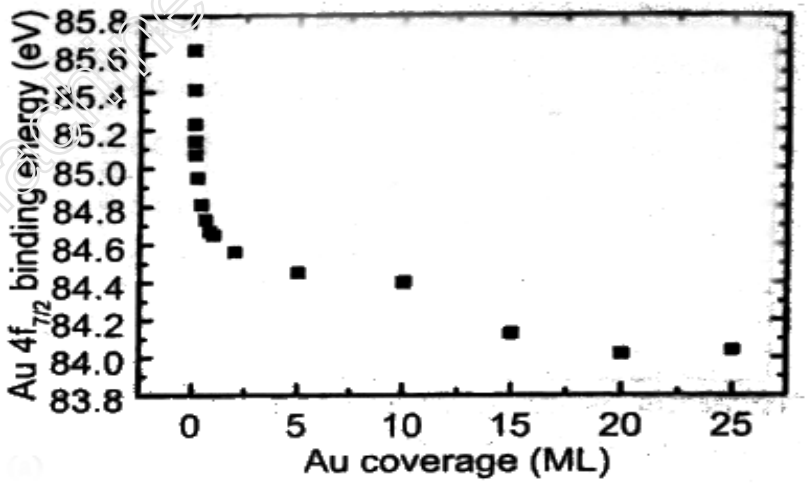

Figure 33. BE change of Au^0 with coverage reported By Goodman [60]

coverage of gold particles obtained from X-ray induced reduction increases from ~0.1 ML to ~4 ML in our study. One point that should be noted is that initial XPS spectrum (t=0) of gold particles deposited from aqueous solution cannot be obtained since X-rays needed to excite photoelectrons will also induce the reduction process. For this reason, initial X-ray photoelectron spectrum where binding energy of Au^0 is measured as 85.31 eV was obtained after approximately 30 minutes of X-ray exposure. This is why Goodman measured a binding energy of 85.80 eV for small gold nanoparticles that is greater than that of our initial binding energy of gold particles (85.31 eV) deposited from aqueous solution. This could have been avoided by having the scans rapidly. As a matter of fact, an initial binding energy of 85.65 eV is obtained after 6 minutes that is the onset of X-ray exposure from another sample whose spectrum is obtained with quick scan. One advantage of our procedure is that it is an in-situ process where reduction and nucleation process occurs at the same time during the course of X-ray reduction. In addition to these, it is observed that the binding energy of gold particles deposited from aqueous solution (0.034% (w/v) of $HAuCl_4$) could not reach the value of the bulk gold (84.00 eV).

Since FWHM also gives information about the particle-size of clusters, FWHM value of gold peak vs time is plotted as shown in Figure 34. Exponential plot gives another evidence of the nucleation process since FWHM of Au^0 peak decreases from 2.25 to 1.85 eV [78].

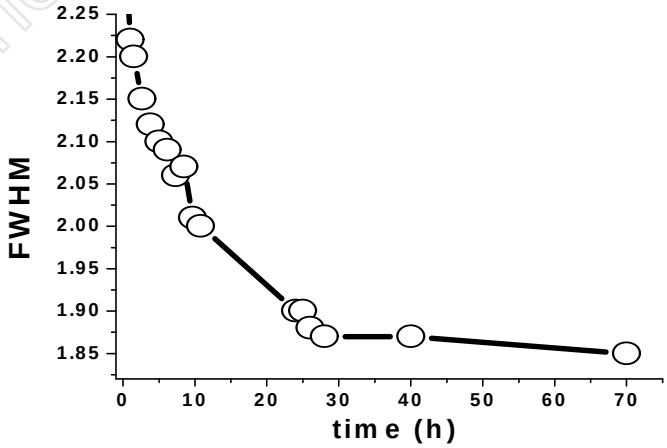

Figure 34. FWHM values for Au^0 $4f_{7/2}$ peak during X-ray exposure

When differential charging occurs during photoemission, energies of atomic levels of sample decrease due to the charge on the sample. The decrease in the energies of core levels results in a decrease in the kinetic energy of photoelectrons and an apparent increase in the binding energy of the atomic levels as stated earlier and shown again in Figure 35.a). In addition, it is observed that the intensity of the detected photoelectrons also increases as illustrated in Figure 35.b), where relative peak ratios of Si^{4+} to Si^{0} and total Au –Au^{3+} and Au^{0}- to Si^{4+} are plotted. It is observed that ratio of the total gold intensity to Si^{4+} intensity ratio increases while Si^{4+} to Si^{0} ratio does not show any significant change. Two factors may contribute to this; increase in Au_{total} / Si^{4+} ratio, (i) gold atoms are migrated to the substrate surface during X-ray induced reduction so that more electrons are emitted without significant attenuation, (ii) the charging also influences the number of electrons emitted. While energies of atomic core levels decrease due to charging, the intensity of photoelectrons also decreases since kinetic energy of photoelectrons decreases. Increase in total Au to Si^{4+} ratio could show the decrease in differential charging of gold layer.

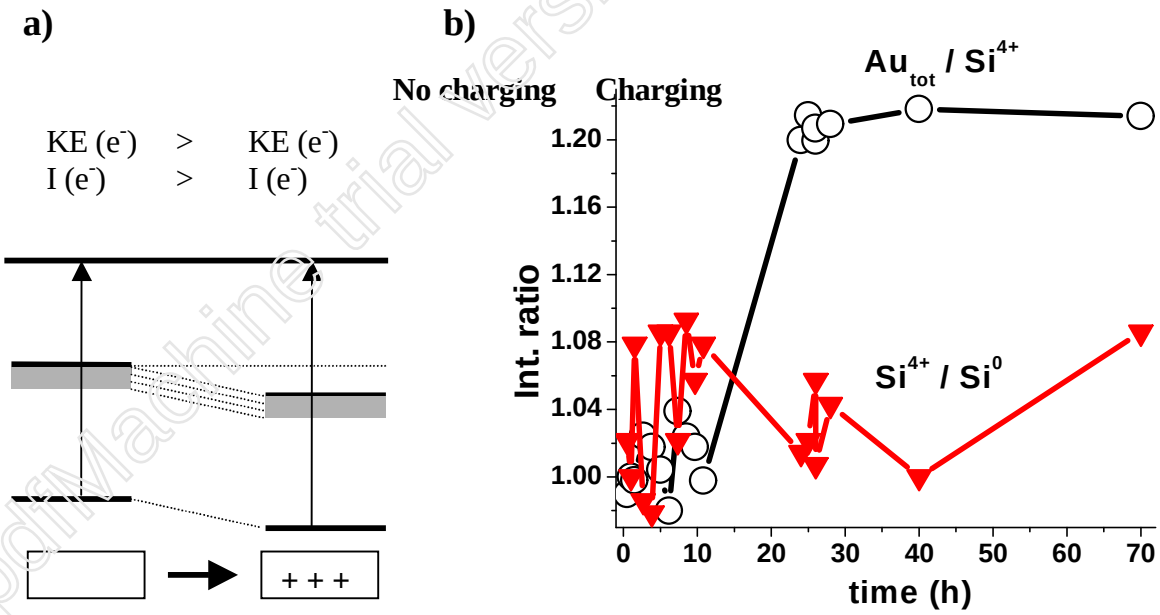

Figure 35. a) Decrease of atomic energy levels due to charging **b)** (Si^{4+}/Si^{0}) and (Au_{tot} / Si^{4+}) peak ratios during X-ray induced reduction of Au^{3+} (peak ratios are normalized to unity initially)

Considering that there should also be an oxidation process and tetrachloroauric acid is used to deposit gold, Cl 2p peak has also been followed during the reduction of Au^{3+}. The Cl 2p peak similarly decreases while Au^{3+} is reduced to its metallic state as shown in Figure 36. Therefore, the redox reaction may be written as:

$$Au^{3+} + 3e^- \rightarrow Au$$

$$2Cl^- \rightarrow Cl_2 + 2e^-$$

$$2Au^{3+} + 6Cl^- \rightarrow 3Cl_2 + 2Au$$

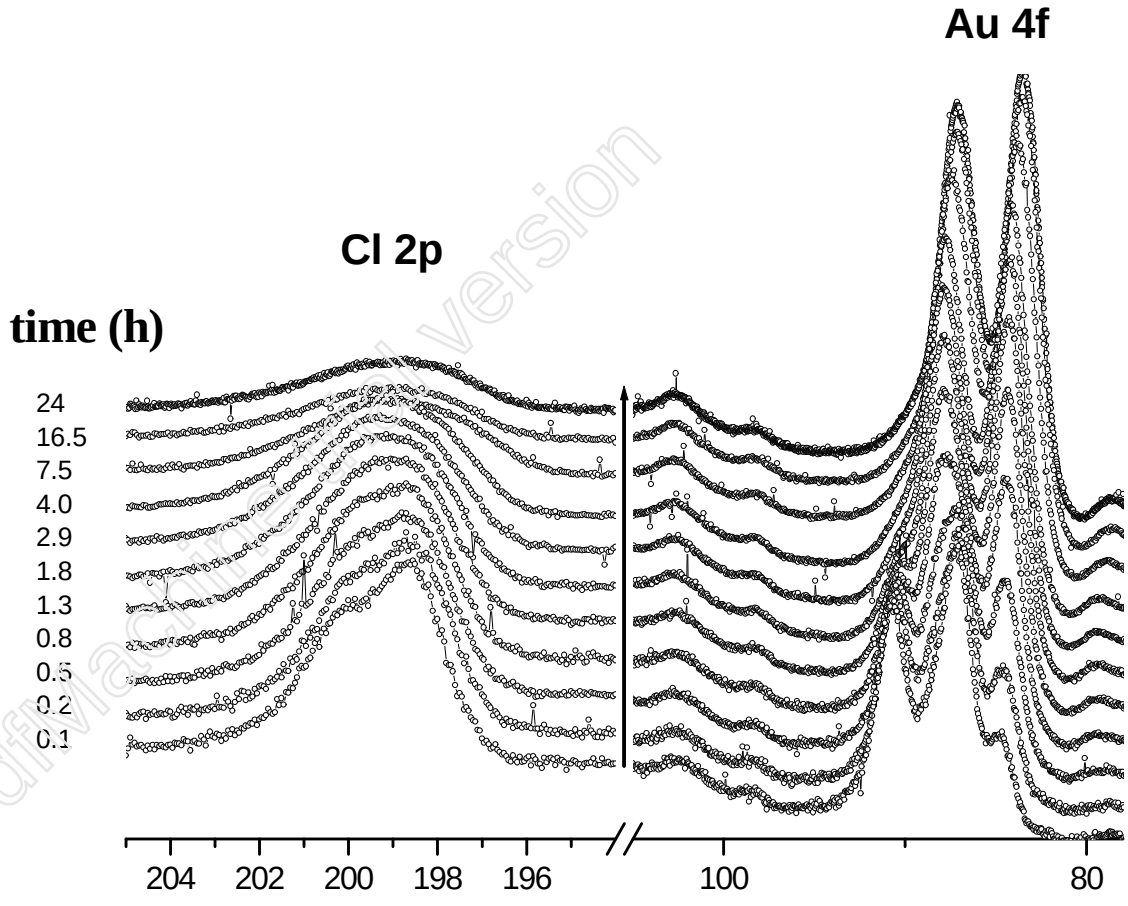

Figure 36. Variation of Cl 2p and Au 4f 7/2 peaks during the course of X-ray exposure

When Au^{3+} is reduced to its metallic state, chloride (2p) peak must also decrease with a similar trend according to the redox reaction written above. Since tetrachloroauric acid is the only source for chloride anion and three chloride anion is oxidised to reduce one gold atom, the intensity of Cl 2p peak should decrease to an intensity ratio of about 1 when Au^{3+} reduction is completed. As shown in Figure 37, a complete reduction of Au^{3+} to Au occurs after 16 hours as chloride concentration decreases to the expected range.

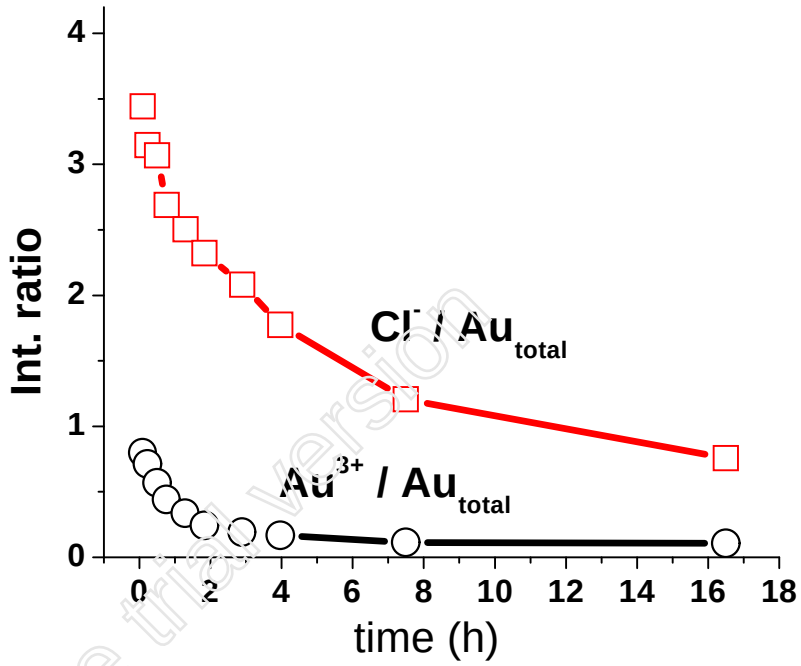

Figure 37. Variation of chloride peak during the course of X-ray exposure

4.2.2 Investigation of the Structure of Gold Clusters Using ARXPS Method

It is possible to have an idea about the structure of gold layer on SiO_2/Si system deposited from aqueous solution using the Angle Resolved XPS (ARXPS) method. As mentioned in the introduction part, theoretical graphs could be calculated for the intensity ratio versus sinΘ of a uniform bilayer system where Θ is the take-off angle. When plots are normalized to 1 at 90^o, it is seen that the increase in the intensity ratio shows a

logarithmic behavior for both SiO_2/Si and Au/SiO_2 systems as given in Figures 38 and 39, respectively.

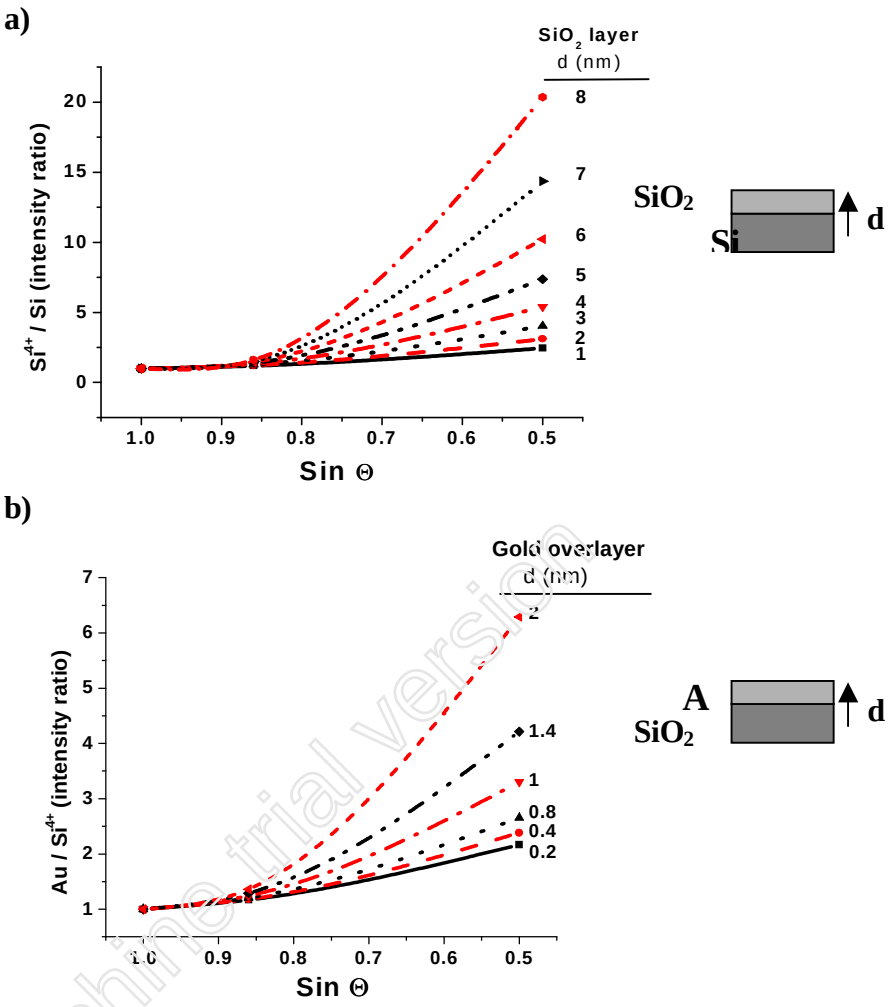

Figure 38. Theoretical graphs plotted sin θ vs intensity ratio, **a)** (Si^{4+} / Si^{0}), **b)** (Au^{0} / Si^{4+})

When this method is applied to gold particles on SiO_2/Si system deposited from aqueous solution, the recorded spectra at three different angles (30^o, 60^o, 90^o) are shown in Figure 39 and the intensity ratio values measured at different angles are tabulated in Table 8.

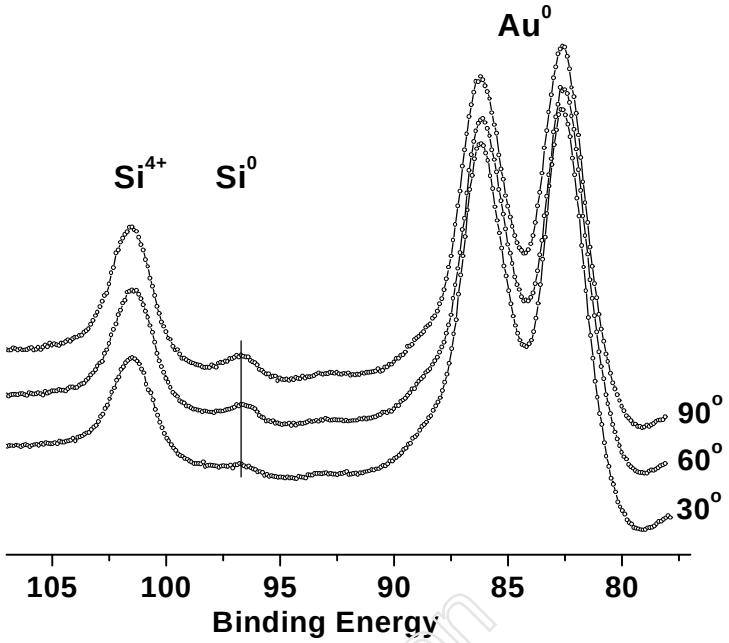

Figure 39. XPS of $Au(AuCl_4^-)/SiO_2/Si$ system at different angles

Table 8. Intensity ratio data for $Au(AuCl_4^-) / SiO_2 / Si$

	Au^0 / Si^{4+}	Au^0 / Si^{4+} (normalized)	Si^{4+} / Si^0	Si^{4+} / Si^0 (normalized)
90^o	4.9	1.0	12.4	1.0
60^o	5.8	1.2	12.7	1.2
30^o	7.1	1.4	31.6	2.6

Decrease in the Au to Si^{4+} and Si^{4+} to Si ratios given in Table 8 is sufficient to establish that Au layer is at the top, SiO_2 is at the middle and Si is at the bottom as expected. To have even more detailed information about the structure of gold particles, different models can be constructed.

It is well established that, upon heating, the silicon oxide layer grows simultaneously and forms a smooth SiO_2 layer on silicon having amorphous structure. In addition, it is also known that gold particles prefer to have island-like 3D-structures rather than a smooth 2D-structure [60]. However, there are no previous studies investigating the structure of gold particles deposited from aqueous solutions. Hence we use Angle Resolved XPS technique and theoretical models for elucidating the structure of $Au/SiO_2/Si$ system. Considering that Au/Si^{4+} and Si^{4+}/Si ratios are 4.9 and 12.4 respectively at 90^o as given in Table 8, which corresponds to theoretical values of 0.22 nm Au layer and 8.6 nm of SiO_2 layer, models shown in Figure 40 which have different percentage coverage of gold are compared with experimental data. First model (100% covered) represents the growth of gold particles two dimensionally (2D-growth), second (50% covered) and third (25% covered) models represent the formation of island-like structures (3D-growth). Height of gold particles increases as the gold coverage decreases so as to keep the amount of gold atoms on the substrate constant.

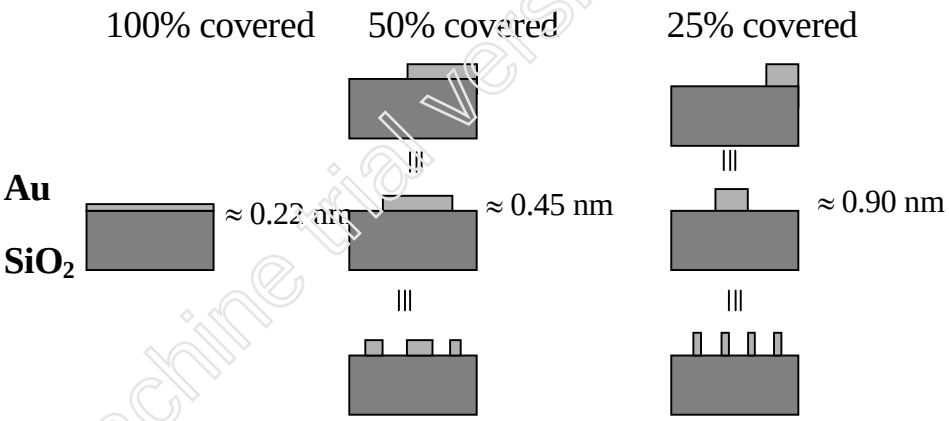

Figure 40. Possible models for $Au(AuCl_4^-)/SiO_2/Si$ system

SiO_2 layer in models that represent 3D gold structures (second and third models) can be grouped into two regions according to the attenuation of the photoelectrons. The first region is the clear SiO_2 layer and the second is that covered with gold overlayer. Since electrons emitted from the second region are totally attenuated by the gold layer and only those emitted from the first region will reach the detector, the number of electrons

emitted from these regions should be calculated separately. For this purpose, theoretical values of Au^0/Si^{4+} ratio are computed and are given in Table 9.

Table 9. Theoretical data of Au^0/Si^{4+} intensity ratio for gold overlayer on SiO_2 for different thicknesses

Au^0 / Si^{4+} ratio	**0.2 nm**	**0.4 nm**	**0.9 nm**	**0.2 nm normalized**	**0.4 nm normalized**	**0.9 nm normalized**
90°	4.28	9.27	26.02	1.00	1.00	1.00
60°	4.99	10.93	32.08	1.17	1.18	1.23
30°	9.27	22.10	81.05	2.17	2.38	3.11

In addition, it is calculated that κ value in equation 6 (pp.8) for Au / SiO_2 system is equal to 23.29 which represents the intensity ratio measured from a sample consisting of same amounts of gold and SiO_2 layer placed side by side, using the data in Table 10.

Table 10. Properties of Au, SiO_2 and Si layer

	Au	**SiO_2**	**Si**
Atomic density (cm^{-3})	0.0978	0.0377	0.0830
Photoionization cross-section (σ)	17.470 (Au 4f)	0.865 (Si 2p)	0.865 (Si 2p)
Attenuation length of photoelectrons (λ, nm)	1.2 [79]	2.7 [80]	2.3 [80]

As an example, when model that has 50% gold coverage is considered, 71.6% of electrons emitted from the SiO_2 layer that is covered with gold layer will reach the detector at 90° according to equation 4 (pp.8). Using this value, a relationship between two different SiO_2 layers could be devised for island models. When the intensity of the gold overlayer is taken as 9.27 considering the intensity ratio for gold overlayer of 0.4 nm

and θ is 90°, the intensity of SiO_2 region under gold overlayer could be assumed to be equal to 1 while the clear surface will be 1/0.716 = 1.397. Since it is 50% covered, total intensity ratio is equal to;

$$I_{Au} / I_{Si} = 9.27 / (1 + 1.397) = 3.87 \quad \text{for } \theta \text{ is } 90^o$$

When the same method is applied for three different angles for both models, Table 11 is obtained where intensity ratio values for three models with different percentage of gold coverage are tabulated.

Table 11. Theoretical intensity ratio data for constructed models

	50% covered model		**25% covered model**		**5% covered model**	
	I_{Au} / I_{Si}	I_{Au} / I_{Si} **normalized**	I_{Au} / I_{Si}	I_{Au} / I_{Si} **normalized**	I_{Au} / I_{Si}	I_{Au} / I_{Si} **normalized**
90°	3.87	1.00	3.54	1.00	1.23	1.00
60°	4.42	1.14	3.96	1.12	1.23	1.00
30°	7.49	1.94	5.61	1.58	1.23	1.00

Comparison of experimental results with theoretical data for the intensity ratio of Au^0 to Si^{4+} indicates that experimental plot fits best to the theoretical plot of 25% gold covered SiO_2/Si substrate as shown in Figure 41. Gold overlayer has a thickness of 4 nm for model having 5% of gold coverage. This prevents most of the photoelectrons emitted from the SiO_2 layer under to reach the detector. For this reason, it is assumed that intensity ratio of Au^0/Si^{4+} is independent of the take-off angle and it is normalized to 1 one for each take-off angle.

Similar calculations could be made using Si^{4+}/Si^0 ratio in addition to using Au^0/Si^{4+} ratio. However, difficulty in measuring Si^0 peak for the smaller angles may give rise to considerable uncertainty.

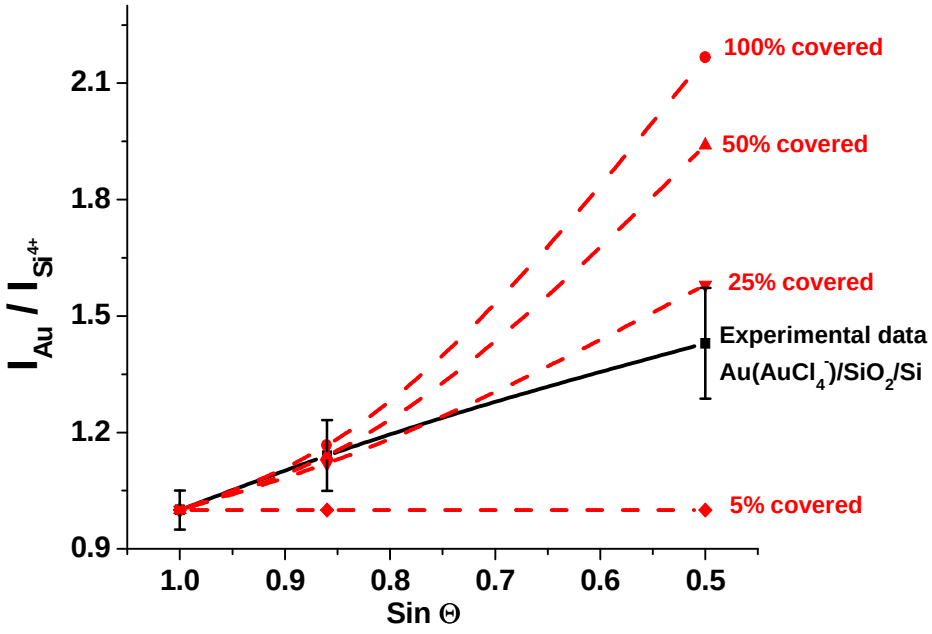

Figure 41. Comparison of intensity ratio (Au to Si^{4+}) between experimental data and constructed models

It is interesting that our oversimplified model is consistent with the claim that Au forms island-like structures on SiO_2/Si when it is deposited from aqueous solution.

4.3. Capped Gold Particles on SiO_2/Si System

4.3.1 Gold Particles with Different Capping Agents on SiO_2/Si System

Capped gold particles can easily be prepared having radius of about 2-50 nm and having partial negative charge around gold atoms due to citrate agent [68-74]. When these particles are deposited on SiO_2/Si system, XPS spectra as given in Figure 42 are recorded and the binding energy values are tabulated in Table 12. Binding energy difference between Si^{4+} and Au^0 is measured as about 19.50 eV for almost all of the samples. When Si^{4+} peak is again correlated to 103.43 eV, binding energy of Au is equal to 84.00 eV which is equal to that of bulk gold. This coincidence may be because of the fact that final state effects due to particle size and charging effect cancel each other. In order to have further information about the origin of these measured chemical shifts, XPS properties of citrate capped nanoparticles on different substrates were also investigated.

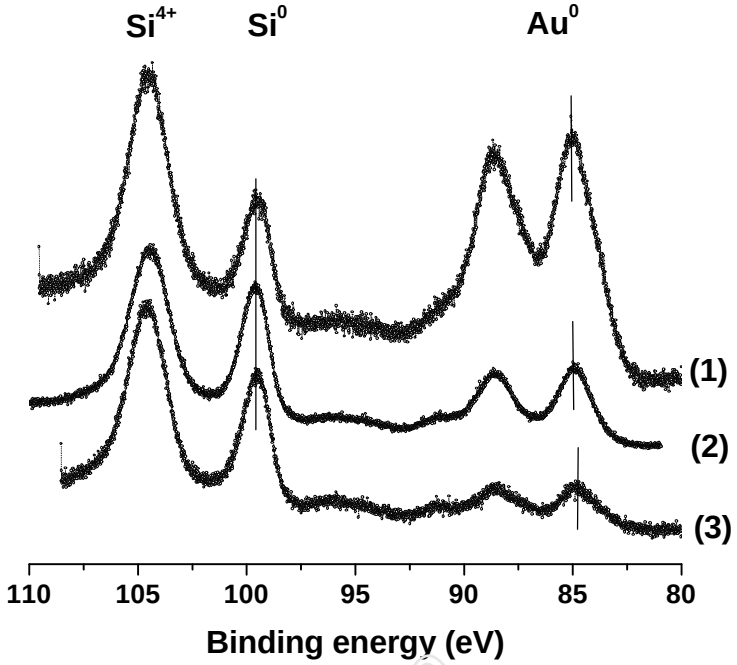

Figure 42. XPS Spectra of sulfate passivated citrate-tannic acid capped **(1)**, citrate capped **(2)** and tannic acid-citrate capped **(3)** gold particles on SiO_2/Si system

Table 12. Binding energy of Au^0 and Si^{4+} of of sulfate passivated citrate-tannic acid capped **(1)**, citrate capped **(2)** and tannic acid-citrate capped **(3)** gold particles on SiO_2/Si system when Si^0 2p peak is correlated to 99.60 eV (Figure 42)

Sample	BE (Si^{4+})	BE (Au^0)	BE (Si^{4+}-Au^0)	Si^{4+} / Si^0	Au^0 / Si^{4+}
(1)	104.60	85.10	19.50	2.6	0.08
(2)	104.40	84.90	19.50	1.8	0.04
(3)	104.60	84.90	19.70	2.0	0.20

4.3.2 Capped Gold Particles on Different Substrates

In order to investigate the effect of the substrate on the binding energy of gold particles, citrate capped gold particles are deposited on different substrates as shown in Figure 43. In addition to SiO_2/Si substrate, quartz composed of SiO_2 units in diamond

structure and glass consisting of sodium, calcium cations and silicates, are used. Measured binding energy difference between Si^{4+} and Au^0 is 19.47 and 19.43 eV for SiO_2/Si and quartz, respectively and decreases to 19.28 eV for the glass substrate. Noting that precision of measuring binding energy difference is better than 0.05 eV, the derived values for quartz and SiO_2/Si system could be assumed to be similar and small binding energy differences are the result of differential charging between gold clusters and oxide layer or the cluster-size or the combination of both of them. When binding energy of Si^{4+} is correlated to 103.43 eV, the binding energy values of gold on quartz and SiO_2/Si system are very close to that of bulk gold, 84.00 eV. The measured shift (0.15 eV) for glass substrate compared to quartz and SiO_2/Si system indicate that substrate type also affects the binding energy difference.

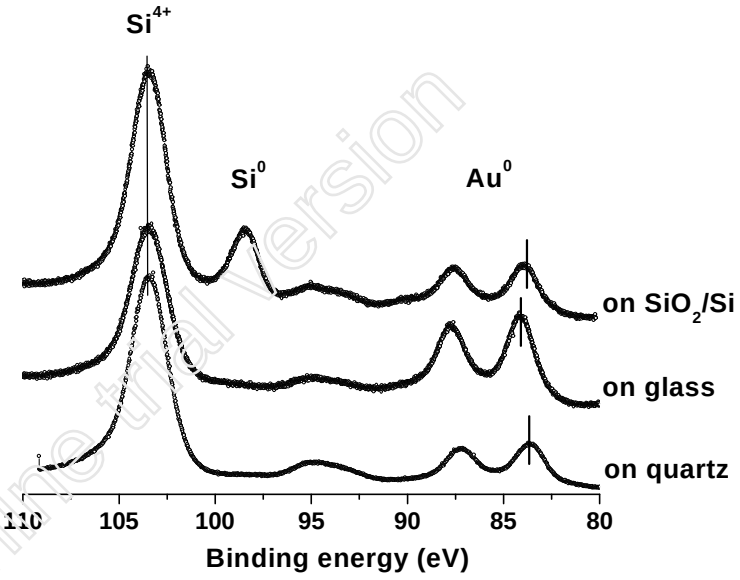

Figure 43. XPS Spectra of citrate capped nanoparticles on SiO_2/Si, on glass and on quartz

4.3.3 Visible and Electrophoresis Studies

As mentioned in the introduction part, the particles-size of gold particles could be followed by their sharp absorption peak at 523 nm [68-74]. Furthermore, it has been reported that capped gold nanoparticles aggregate when they are deposited on a substrate.

To investigate whether capped gold nanoparticles aggregate permanently on quartz and glass, Vis-properties of capped gold particles in aqueous solution, deposited on the substrate and those after transferred from the substrate back to aqueous solution are compared as shown in Figure 45. Absorption peak at 523 nm shifts to higher wavelength when solution is deposited on a solid substrate that is indicative of aggregation process and shifts back to 523 nm when they are transferred back to the aqueous solution. This fact shows that shift is only due to a soft aggregation which is reversible rather than a coagulation process that is irreversible. Electrophoresis method can also be used to investigate this property of capped gold particles since particles travel in the gel according to their sizes and charges. For this purpose, solutions of gold nanoparticles having absorption peaks of different wavelengths (~523-530 nm) have been prepared where Vis-spectra are displayed in Figure 44. A similar trend is also observed in electrophoresis as shown in Figure 46. The citrate capped gold nanoparticles have partial negative charge since they move from cathode (-) to anode (+). The other point is that sample(A) having the absorption peak of shortest wavelength travels the longest distance. As the wavelength of absorption peak increases indicating the increase in particle-size, the distance traveled (in the same period) decreases. A similar correlation could not be observed between gold nanoparticles with different capping agents. This may because of the fact that the charge on capping agents has a very strong pH dependence of the medium.

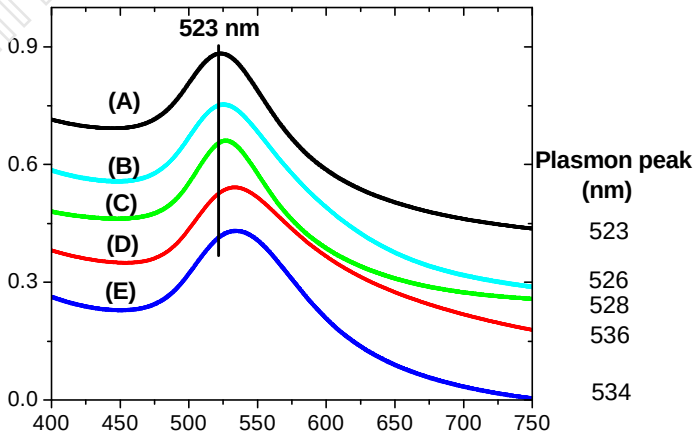

Figure 44. Vis-absorption spectra of citrate capped gold particles with different particle sizes (Samples were prepared with same method explained in experimental part)

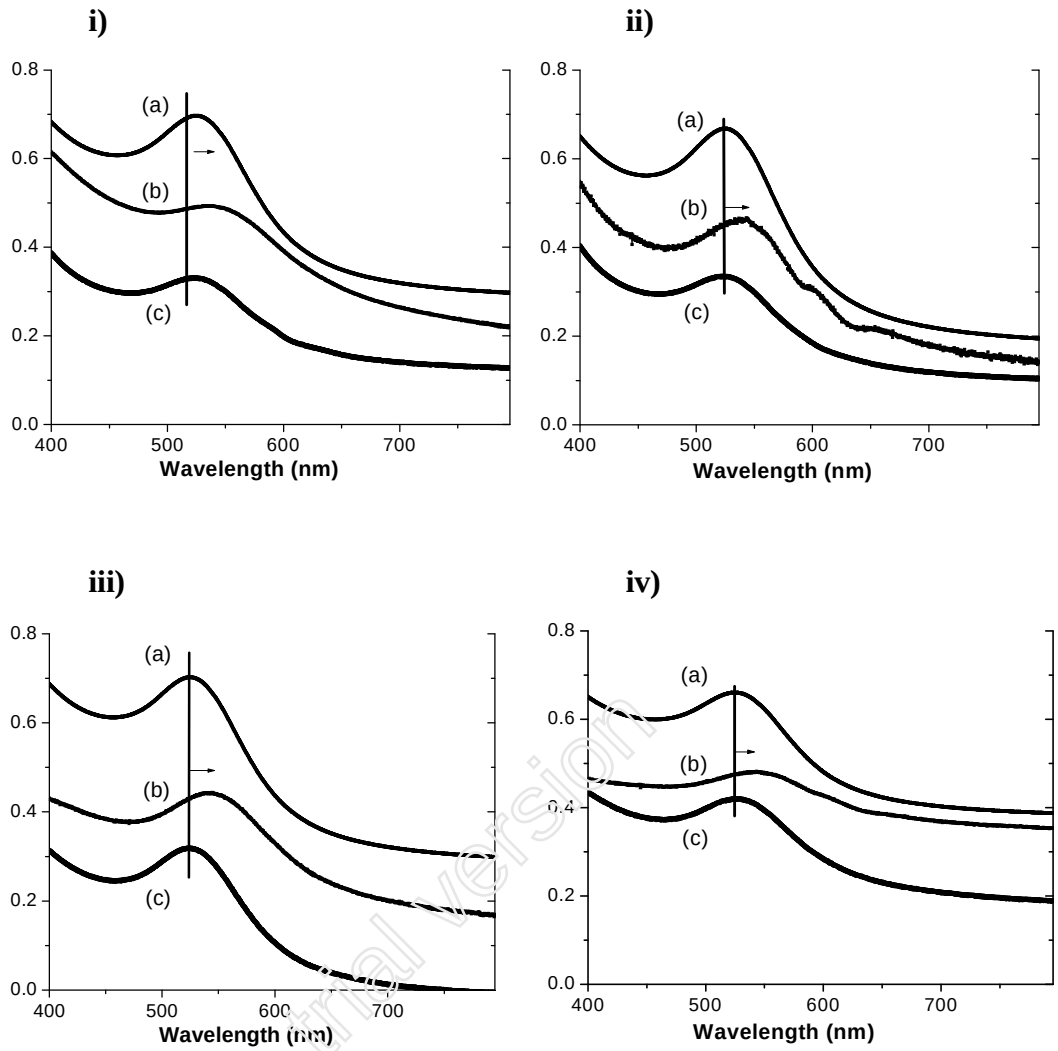

Figure 45. i) Visible spectra of citrate capped gold particles (a) in aqueous solution (as prepared), (b) deposited on quartz, and (c) after transferring the deposited nanoclusters back into the aqueous solution, **ii)** Visible spectra of citrate capped gold particles (a) in aqueous solution (as prepared), (b) deposited on glass, and (c) after transferring the deposited nanoclusters back into the aqueous solution, **iii)** Visible spectra of sulfate passivated citrate capped gold particles (a) in aqueous solution (as prepared), (b) deposited on quartz, and (c) after transferring the deposited nanoclusters back into the aqueous solution, **iv)** Visible spectra of sulfate passivated citrate capped gold particles (a) in aqueous solution (as prepared), (b) deposited on glass, and (c) after transferring the deposited nanoclusters back into the aqueous solution

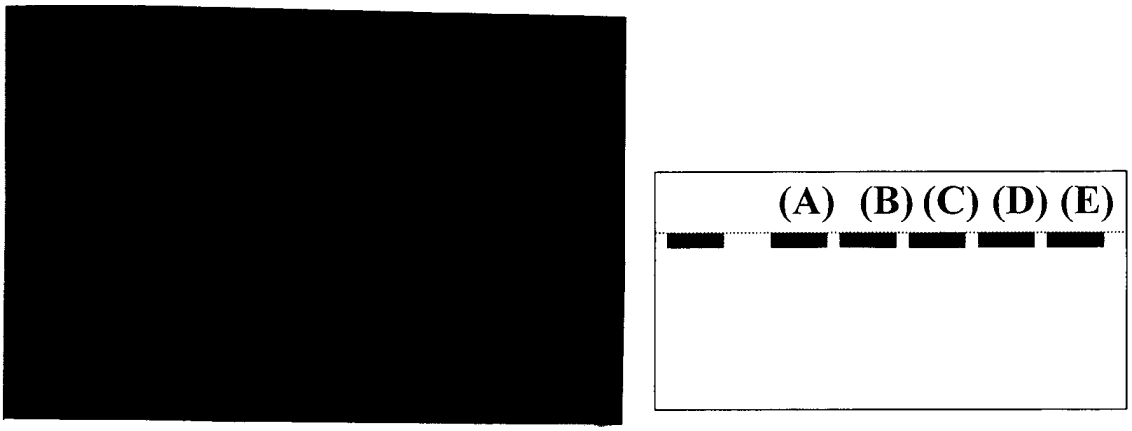

t = 0 min

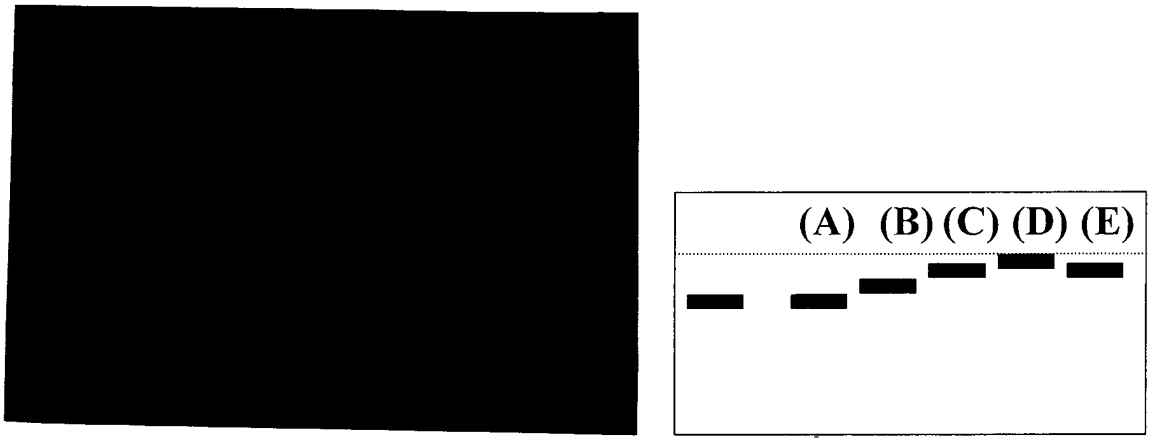

t = 5 min

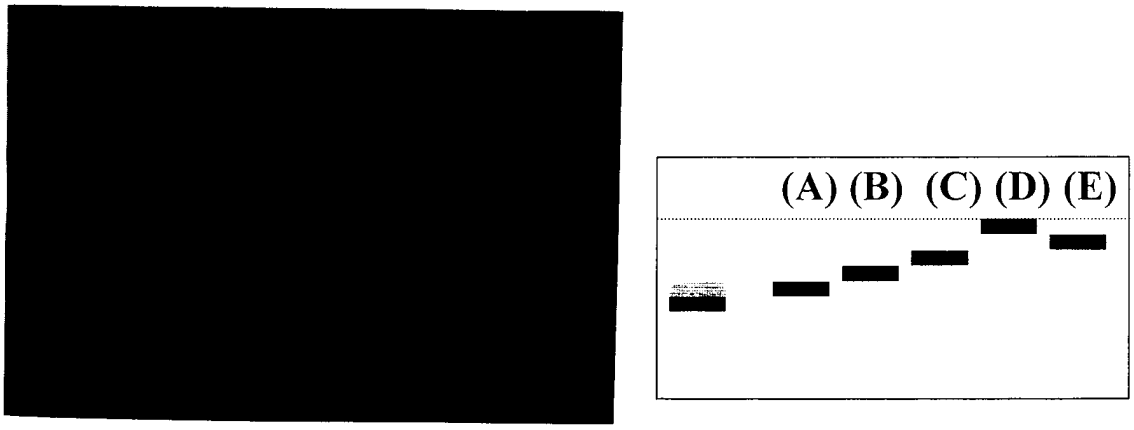

t = 10 min

Figure 46. Pictures of electrophoresis when capped gold particles are allowed to run in the gel at V = 100V (sample having a color of blue is the marker)

4.4 Chemically Reduced Gold Particles on SiO_2/Si System

Gold particles are also reduced chemically by $NaBH_4$ in aqueous solution and then deposited on SiO_2/Si substrate where an XPS spectrum is shown in Figure 47.

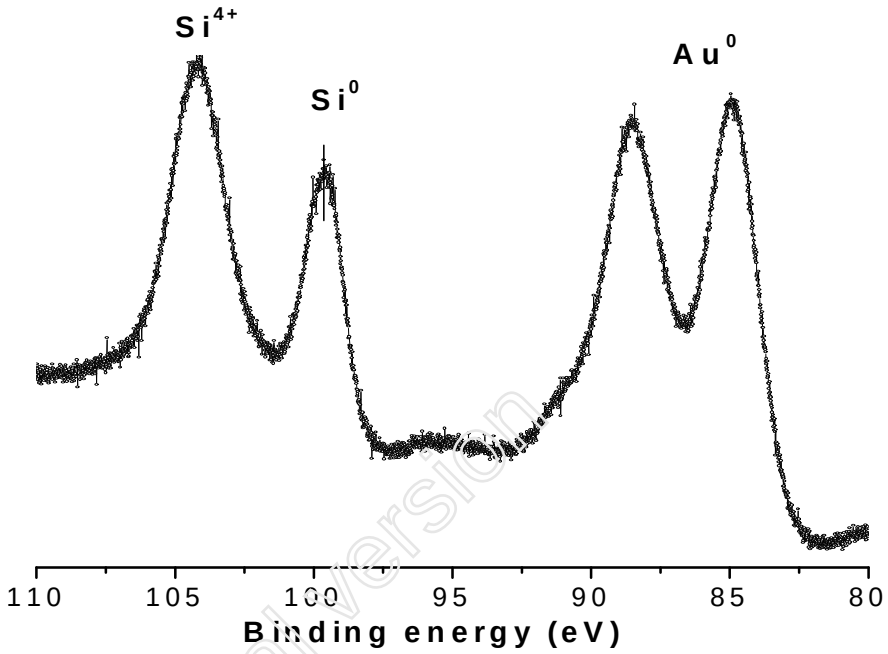

Figure 47. XPS Spectrum of gold particles reduced chemically by $NaBH_4$ deposited on SiO_2/Si system, Si^0 peak is correlated at 99.60 eV, Au/Si^{4+} ratio is 0.1, Si^{4+}/Si^0 ratio is 2.0.

Binding energy difference between Au^0 and Si^{4+} is measured as 19.30 eV, which corresponds to 84.15 eV close to the binding energy of bulk gold. Since there is no reagent that prevents the aggregation of gold particles to control their particle-size, gold particles could easily aggregate. This may be the reason why gold particles reduced chemically by $NaBH_4$ have binding energy close to that of bulk gold.

4.5 Gold Particles on SiO_2/Si System with Different SiO_2 Thickness Values

4.5.1 Au (aq) System with Different SiO_2 Thickness Values

When gold is deposited from aqueous solution on SiO_2/Si with different oxide layers, it is observed that Au $4f_{7/2}$ peak shifts to higher binding energy with the increase in Si^{4+} 2p peak as shown in Figure 48. Spectra are correlated to Si 2p peaks (99.6 eV) to show these shifts clearly.

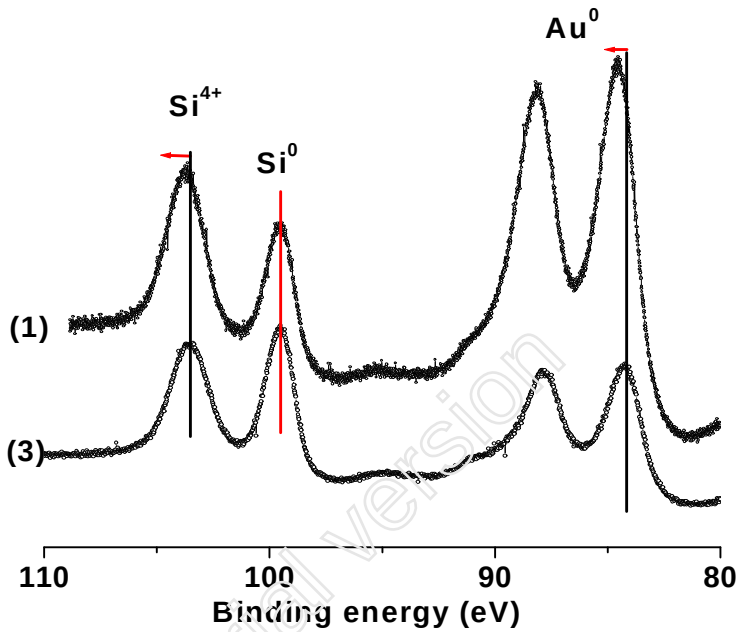

Figure 48. Au particles deposited from aqueous solution on SiO_2/Si having different thicknesses of SiO_2 layer

Although a shift in Au $4f_{7/2}$ peak is observed as the thickness of SiO_2 layer changes, binding energy difference between Au^0 and Si^{4+} stays constant as given in Table 13 indicating that charging behavior of gold particles is similar to that of SiO_2 layer. Moreover, binding energy of Au^0 is approximately equal to 84.40 eV when Si^{4+} peak is correlated to 103.43. Despite the variation in Au^0/Si^{4+} ratio, it does not approach the binding energy of bulk gold, 84.00 eV. This may be due to the structure of gold particles or this is the result of the fact that insufficient amount of gold is deposited on SiO_2/Si to have bulk-like gold structure. From Figure 33, a gold coverage up to 20 ML is needed to

obtain bulk-like properties. Sample (3) having the largest Au/Si^{4+} intensity ratio has a theoretical gold coverage of about 0.20 nm. When one assumes the radius of gold atom as 145 pm, it can be calculated that only a gold coverage of 0.7 ML was prepared which supports the suggestion that there is insufficient amount of gold to have bulk-like properties.

Table 13. Mesaured binding energies together with intensity ratio values for samples having different SiO_2 thickness values (**(1)**, **(2)**, **(3)** are samples prepared in similar conditions having oxide layers with different thickness values and SiO_2/Si system was allowed to stay in aqueous gold solution for various durations)

Sample	Si^{4+}	Au	BE (Si^{4+}-Au)	Si^{4+} / Si	Au / Si^{4+}
(1)	103.60	84.70	18.90	1.5	0.02
(2)	103.60	84.60	19.00	1.5	0.40
(3)	103.50	84.40	19.10	1.1	0.22
(4)	103.40	84.40	19.00	1.0	0.60
(5)	103.50	84.40	19.10	0.3	0.05

4.5.2 Au (capped with citrate) System with Different SiO_2 Thickness Values

Binding energy of capped gold particles shifts similar to binding energy of SiO_2 layer as depicted in Figure 49 and Table 14.

Table 14. Mesaured binding energies together with intensity ratio values for samples having different SiO_2 thickness values (**(6)**, **(7)**, **(8)** and **(9)** are samples prepared in similar conditions having oxide layer with different thicknesses and SiO_2/Si system was allowed to stay in aqueous gold solution for various durations)

Sample	Si^{4+}	Au	BE (Si^{4+}-Au)	Si^{4+} / Si	Au / Si^{4+}
(6)	104.60	85.10	19.50	4.5	0.02
(7)	104.40	84.90	19.50	1.8	0.04
(8)	104.10	84.50	19.60	1.1	0.02
(9)	103.80	84.20	19.60	1.0	0.02

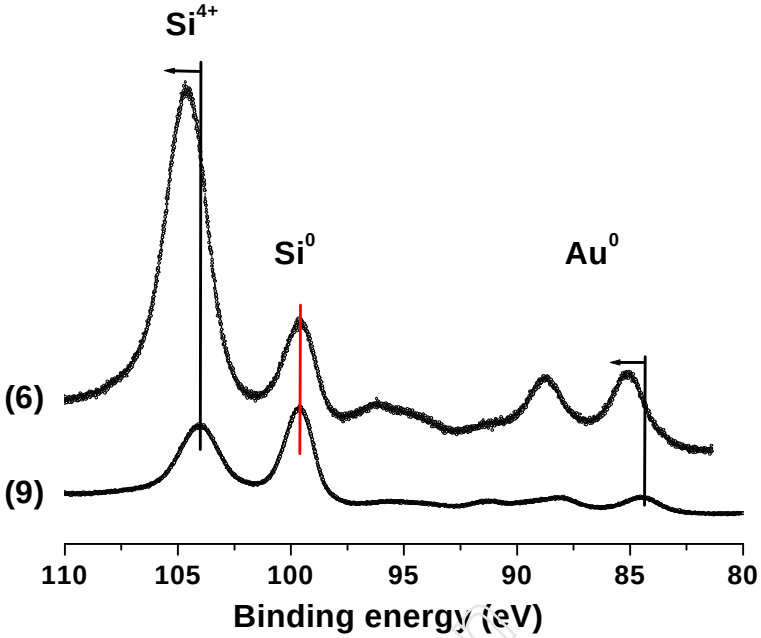

Figure 49. Citrate capped Au particles on SiO_2/Si substrates with different thickness values

Furthermore, it can be concluded that binding energy difference is larger than those deposited from aqueous solution considering the data in Table 14. It is also remarkable that binding energy difference is independent on the thickness of SiO_2 layer and gold coverage.

4.5.3 Au (chemically reduced) System with Different SiO_2 Thickness Values

Deposition of chemically reduced gold particles on SiO_2/Si systems having different thickness of SiO_2 layer gave similar results like other gold particles. Measured binding energies tabulated in Table 15 and shown in Figure 50 indicate that binding energy difference between gold and SiO_2 is large compared to gold particles deposited from aqueous solution.

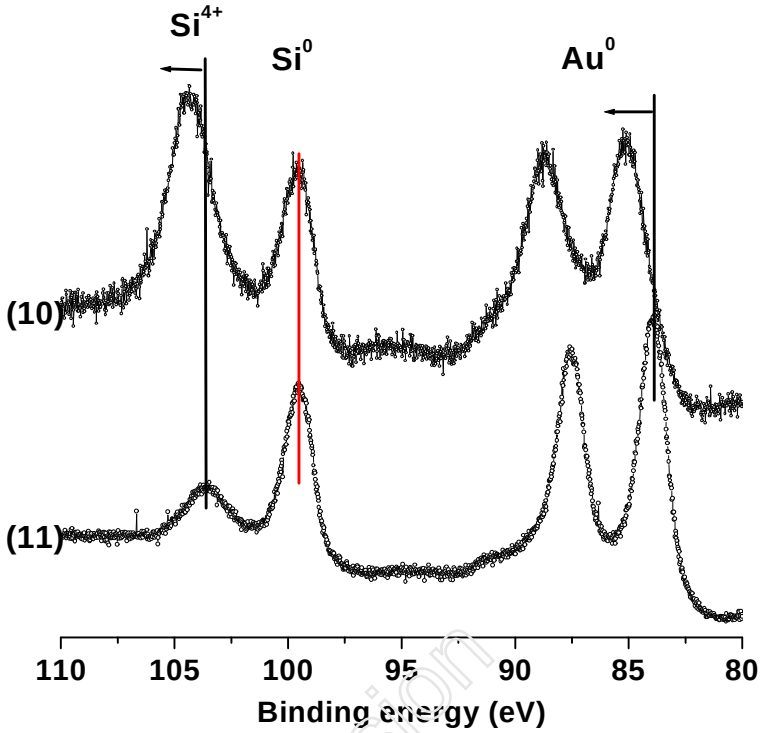

Figure 50. Chemically reduced Au particles on SiO_2/Si substrates with different thickness values

Table 15. Mesaured binding energies together with intensity ratio values for samples having different SiO_2 thickness values (**(10)** and **(11)** are samples prepared in similar conditions having oxide with different thickness values and SiO_2/Si system was allowed to stay in aqueous gold solution for various durations)

Sample	Si^{4+}	Au	BE (Si^{4+}-Au)	Si^{4+} / Si	Au / Si^{4+}
(10)	104.20	85.10	19.10	2.0	0.1
(11)	103.50	84.20	19.30	0.6	0.3

Although binding energy of Si^{4+} 2p peak changes about 0.70 eV, binding energy difference between Si^{4+} 2p and Au $4f_{7/2}$ peak changes about only 0.20 eV indicating that both peaks shift to higher binding energy together.

4.6 Application of an External Bias

Application of external bias to the sample causes changes in the binding energy of Si^{4+} peak as explained in the introduction part. When spectra are correlated according to Si^0 2p peak, positive voltage causes a decrease in binding energy of Si^{4+} peak, and negative voltage causes an increase. When the same procedure is applied to gold particles on SiO_2/Si sample, a similar shift is also observed in Si^{4+} 2p peak, in addition, there occurs a similar shift in Au $4f_{7/2}$ peak as shown in Figure 51. However, the measured binding energy difference between gold and Si^{4+} peaks stays constant as given in Table 16.

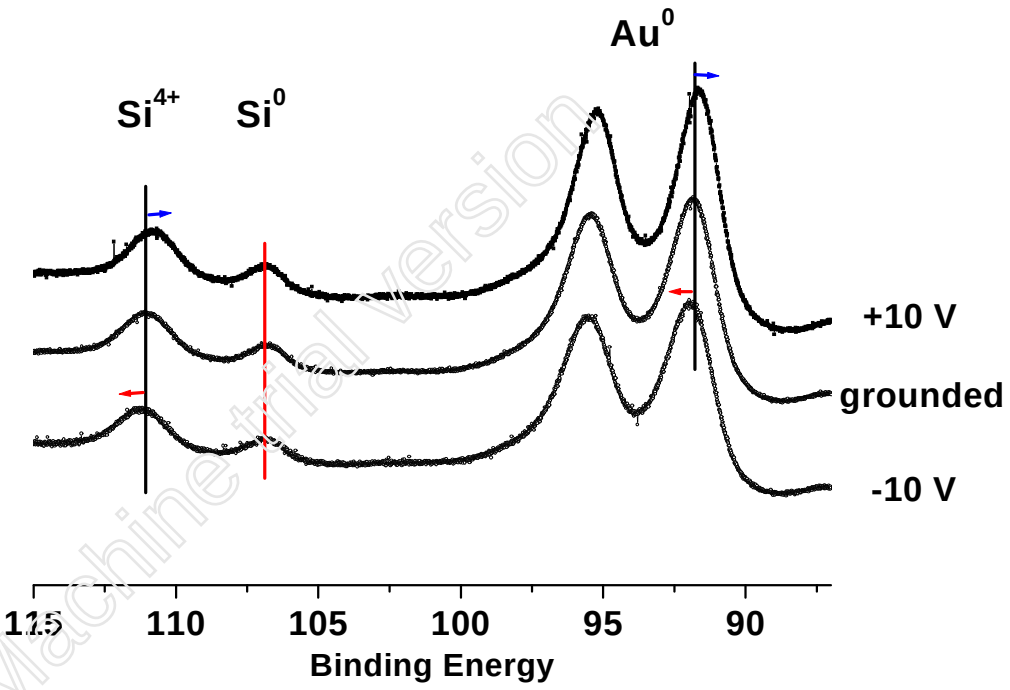

Figure 51. XPS Spectra of Au ($AuCl_4^-$)/SiO_2/Si system when DC-Bias is applied

Results obtained for other types of gold particles are also given in Table 16. Although binding energy difference between Si^{4+} and Si^0 changes about ~0.70 eV, binding energy difference between Si^{4+} and Au^0 changes only about ~0.20 eV when DC bias is applied.

This little change compared to the binding energy difference between Si^{4+} and Si^{0} for each type of gold cluster supports the suggestion that the measured chemical shift of gold and SiO_2 layer has the same origin and gold layer behaves similar to the SiO_2 layer.

Table 16. Binding energy values when external bias is applied to $Au/SiO_2/Si$ system

	Si^{4+}	Au	BE (Si^{4+}-Au)	Si^{4+} / Si	Au / Si^{4+}
Gold particles obtained from aqueous solution					
+10 V	103.45	84.50	18.95		
Grounded	103.60	84.70	18.90	1.7	0.17
-10 V	103.90	84.90	18.90		
Gold particles chemically reduced by $NaBH_4$					
+10 V	103.85	84.50	19.35		
Grounded	104.20	85.10	19.10	2.0	0.10
-10 V	104.50	85.20	19.30		
Citrate capped gold particles					
+10 V	104.30	84.90	19.40		
Grounded	104.60	85.30	19.30	2.3	0.30
-10 V	104.80	85.50	19.30		

4.7 Measurement of the Auger Parameter

One remarkable feature of the Auger Parameter is that it is independent of the binding energy changes resulting from charging effects. Since difference between the binding energies of two electrons that are emitted from the same sample is taken to calculate the Auger Parameter, shifts of two peaks occuring in the same direction with the same amount cancel each other.

As given Table 17, the Auger Parameter remains constant while peak ratio of Au^{0} to Si^{4+} changes from 2.33 to 1.61 indicating that Auger Parameter is independent on peak ratio and the angle of detection.

Table 17. Auger Parameter data for Angle Resolved XPS technique

Electron take-off angle	**Peak ratio (Au / Si^{4+})**	**Peak ratio (Si^{4+} / Si)**	**Auger parameter difference (Si^{4+} - Si)**
30°	2.33	7.27	3.86
90°	1.61	3.97	3.83

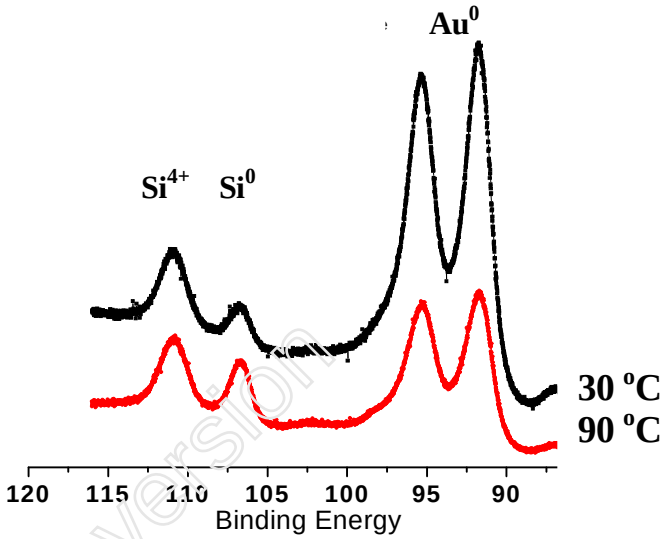

Figure 52. Spectra of sample measured using Angle Resolved XPS technique at 90° and 30°

Data tabulated in Table 18 is obtained when one calculates Auger Parameter of a sample consisting of gold particles on SiO_2/Si system. Although binding energy difference between Si^{4+} and Si peaks changes about 400 meV at ± 10V, Auger parameter changes only about 60 meV, which is approximately in error range of XPS (50 meV). The small change in Auger Parameter value compared to the change of difference in binding energies of Si^{4+} and Si peaks indicates that the chemical shift measured during the application of DC-Bias is solely due to charging.

Table 18. Measured Si 2p binding and Si_{KLL} kinetic energies of the sample containing gold particles on SiO_2/Si system deposited from aqueous solution, together with the Auger Parameters (Si^0 2p peak is correlated to 99.50 eV and Si^0_{KLL} peak is correlated to 1616.40 eV, AP is the abbreviation of Auger Parameter)

	Si 2p BE (eV)		**Si_{KLL} KE (eV)**		**AP**		
	Si^{4+}	ΔBE	Si^{4+}	ΔKE	Si^{4+}	Si^0	ΔAP
+10 V	103.34	3.84	1608.63	-7.77	1711.97	1715.90	3.93
Grnd	103.63	4.13	1608.41	-7.99	1712.04	1715.90	3.86
-10 V	103.74	4.24	1608.24	-8.16	1711.98	1715.90	3.92

5. CONCLUSIONS

The main emphasis of this work is to elucidate the factors affecting the measured chemical shift of Au 4f peak on the SiO_2/Si substrate. It is well-known that binding energy difference between Si^{4+} and Si^0 increases as the oxide thickness increases. It is also observed that binding energy of Au^0 shifts similar to Si^{4+} peak so that binding energy difference between Au^0 and Si^{4+} remains constant as the oxide thickness changes. Similar trend is also observed upon application of an external bias, supporting our finding that SiO_2 layer could be chosen as reference point rather than Si substrate. Using gold layers prepared by PVD method, the binding energy Si^{4+} 2p has been assigned to 103.43 ± 0.05 eV.

Au particles have mostly been deposited from aqueous solution. Investigations performed with Au particles deposited from aqueous solution have shown that Au^{3+} is reduced during X-ray exposure since Au^0/Si^{4+} peak ratio increases exponentially. Since the binding energy of Au^0 also decreases exponentially and approaches to that of bulk gold indicating possibly a nucleation process, it is concluded that reduction and nucleation processes occur at the same time. Exponential decrease in FWHM value of Au^0 has given another evidence to the nucleation and growth of Au^0 particles. It is also observed that total Au –Au^{3+} and Au^0- to Si^{4+} peak ratio increases during X-ray exposure which may be attributed to the decrease in differential charging of Au^0 particles resulting in an increase in the number of photoelectrons emitted. Angle Resolved XPS method, which is used to obtain information about the structure of gold particles deposited from aqueous solution, supported the idea that Au^0 particles prefer to grow three-dimensionally (island-like model) rather than two-dimensionally. But in all cases, the measured binding energy of the Au^0 particles (ca. 84.30 ± 0.05 eV) cannot reach the bulk value (84.00 ± 0.05 eV).

Capped Au^0 particles and chemically reduced ($NaBH_4$) gold particles have also been deposited on SiO_2/Si system. Similar to the aqueous system, the binding energy difference between Au^0 and Si^{4+} does not change significantly while that between Si^{4+} and Si^0 changes due to oxide thickness. The binding energy of capped gold particles is

determined as 84.00 ± 0.05 eV, close to that of bulk gold. This coincidence for capped gold particles may be due to the fact that final state effects (particle-size) and charging effect cancel each other. When citrate capped Au^0 particles have also been deposited on quartz and glass, a shift of about 0.15 eV has been observed that may be a result of differential charging between gold layer and the substrate or the cluster-size or the combination of them. Vis-absorption and electrophoresis studies have complemented our findings that capped gold particles aggregate reversibly (i.e. they do not coagulate) when they are deposited on SiO_2/Si system and transferred back to solution and their partial negative charge which may contribute to the measured chemical shift.

The derived Auger Parameters have also given evidence that the chemical shift measured during the application of external bias is solely due to charging.

Effect of substrate to gold particles was discussed throughout this thesis. For further studies, intensity, FWHM and binding energy parameters of Si^{4+} peak belonging to SiO_2/Si and Au/ SiO_2/Si systems may be compared to investigate the effect of gold particles to the substrate.

6. REFERENCES

[1] G. F. Cerofoni, L. Meda, "Physical Chemistry of, in and on Silicon", *Springer Verlag*, New York, **1989**

[2] F. J. Grunthaner, P. J. Grunthaner, R. P. Vasquez, B. F. Lewis, J. Maserjian, "High Resolution X-ray Photoelectron Spectroscopy as a Probe of Local Atomic Structure: Application to Amorphous SiO_2 and the Si-SiO_2 Interface", *Phys. Rev. Lett.* 43(22), 1683-1686, **1979**

[3] K. Z. Zhang, J. N. Greeley, M. M. Banaszak Holl, "The Role of Extra Atomic Relaxation in Determining Si 2p Binding Energy Shifts at Silicon/Silicon Oxide Interfaces", *J. Appl. Phys.* 82(5), 2298-2307, **1997**

[4] F. R. McFeely, K. Z. Zhang, M. M. Banaszak Holl, S. Lee, J. E. Bender IV, "An Inquiry Concerning the Principles of Si 2p Core-level Photoemission Shift Assignments at the Si/SiO_2 Interface", *J. Vac. Sci. Technol. B* 14(4), 2824-2831, **1996**

[5] S. Iwata, A. Ishizaka, "Electron Spectroscopic Analysis of the SiO_2/Si System and Correlation with Metal-oxide-Semiconductor Device Characteristics", *J. Appl. Phys.* 79 (9), 6653-6713, **1996**

[6] A. Pasquarello, M. S. Hybertsen, R. Car, "Theory of Si(01)-SiO_2 Interface", *Phys. Rev. B*, 53(16), 10942-10950, **1996**

[7] K. Z. Zhang, M. M. Banaszak Holl, "Extra-atomic Relaxation and Core-level Binding Energy Shifts at Silicon/Silicon Oxide Interfaces: Effects of Cluster Size on Physical Models", *J. Phys. Chem. B*, 102, 3930-3935, **1998**

[8] H. Kobayashi, T. Kubota, H. Kawa, Y. Nakato, M. Nishiyama, "Oxide Thickness Dependence of Energy Shifts in the Si 2p levels for the SiO_2/Si structure, and its Elimination by a Palladium Overlayer", *Appl. Phys. Lett.*, 73(7), 933-935, **1998**

[9] R. Browning, M. A. Sobolewski, C. R. Helms, "Effect of Electrostatic Screening on Energy Positions of Electron Spectra near SiO_2/Si Interfaces", *Phys. Rev. B*, 38(18), 13407-13410, **1988**

[10] G. F. Cerofolini, C. Galati, L. Renna, "Accounting for Anomalous Oxidation States of Silicon at the Si/SiO_2 Interface", *Surf. Interface Anal.*, 34, 577-582, **2002**

[11] B. Ulgut, S. Suzer, "XPS Studies of SiO_2/Si System under External Bias", *J. Phys. Chem. B*, 107, 2939-2943, **2003**

[12] F. Liebau, "Structural Chemistry of Silicates, Structure, Bonding and Classification", *Springer Verlag*, Berlin **1985**

[13] V. K. Adamchuk, A. M. Shikin, "Si – Noble Metal (Au, Cu, Ag) Interface Formation Studies by AES", *J. Elect. Rel. Phen.*, 52, 103-112, **1990**

[14] L. Guczi, D. Horvath, Z. Paszti, L. Toth, Z. E. Horvath, A. Karacs, P. Geto, "Modeling Gold Nanoparticles: Morphology, Electron Structure, and Catalytic Activity in CO Oxidation", *J. Phys. Chem. B*, 104, 3182-3193, **2000**

[15] T. V. Choudhary, D. W. Goodman, "Oxidation Catalysis by Supported Gold Nanoclusters", *Topics in Catalysis*, 21, 25-34**, 2002**

[16] G. Battistoni, G. Mattogno, R. Zanoni, L. Naldini, "Characterisation of Some Gold Clusters by X-ray Photoelectron Spectroscopy", *J. Elec. Spec. Rel. Phen*. 28(1), 23-32, **1982**

[17] C. Battistoni, G. Mattogno, D. M. P. Mingos, "Characterisation of Some Gold Cluster Compounds by X-ray Photoelectron Spectroscopy", *J. Elec. Spec. Rel. Phen* 33(2), 107-114, **1984**

[18] CRC Handbook of Physics and Chemistry, *CRC Press*, 75th Edition**,** Cleveland**,** Ohio, **1995**

[19] P. S. Peercy, "The Drive to Miniaturization", *Nature,* 406, 1023-1026, **2000**

[20] M. Schulz, "The End of the Road for Silicon", *Nature*, 399, 729-730, **1999**

[21] D. Briggs, M. P. Seah, *Practical Surface Analysis*, John Wiley&Sons, Chichester, **1996**

[22] S. Suzer, "Multiplets in Atoms and Ions Displayed by Photoelectron Spectroscopy", *J. Chem. Edu.*, 59, 814-815, **1982**

[23] J. F. Moulder, W. F. Stickle, P. E. Sobol, K. D. Bomben, Handbook of X-Ray Photoelectron Spectroscopy, *Perkin Elmer Corporation*, **1992**

[24] A. Ishizaka, S. Iwata, "Si-SiO2 Interface Characterisation from Angular Dependence of X-ray Photoelectron Spectra", *Appl. Phys. Lett.*, 36(1), 71-73, **1980**

[25] D. F. Mitchell, K. B. Clark, J. A. Bardwell, W. N. Lennard, G. R. Masoumi, I. W. Mitchell, "Film Thickness Measurements of SiO_2 by XPS", *Surf. Interface Anal.*, 21, 44-50, **1994**

[26] J. E. Fulghum, "Determination of Overlayer Thickness by Angle-resolved XPS: A Comparison of Algorithms", *Surf. Interface Anal.*, 20, 161-173, **1993**

[27] P. Kappen, K. Reihs, C. Seidel, M. Voetz, H. Fuchs, "Overlayer Thickness Determination by Angular Dependent X-ray Photoelectron Spectroscopy (ADXPS) of rough Surfaces with a Spherical Topography", *Surf. Sci.*, 465, 40-50, **2000**

[28] M. F. Ebel, "Evaluating Ratio Data For the Determination of Reduced Thicknesses by XPS", *Surf. Interface Anal.*, 3(4), 149-152, **1981**

[29] M. F. Ebel, "The Significance of Reduced Thicknesses Determined by XPS using the Variable Take-off Angle Technique", *Surf. Interface Anal.*, 3(4), 173-175, **1981**

[30] R. Jisl, "Restoration of the Depth-Concentration Profile from the Angle-resolved Relative Intensities of X-ray Photoelectron Spectra", *Surf. Interface Anal.*, 15, 719-726, **1990**

[31] L. B. Hazell, I. S. Brown, F. Freisinger, "A Model for Determining the Composition of Layer Structured Samples Using XPS Electron Take-off Angle Experiments", *Surf. Interface Anal.* 8, 25-31, **1986**

[32] M. Schaepkens, G. S. Oehrlein, C. Hedlund, L. B. Jonsson, H. Blom, "Selective SiO_2-to-Si_3N_4 Etching in Inductively Coupled Fluorocarbon Plasmas: Angular Dependence of SiO_2 and Si_3N_4 Etching Rates ", *J. Vac. Sci. Technol. A* 16(6), 3281-3284, **1998**

[33] C. Birer, S. Sayan, S. Suzer, A. Aydinli, "XPS Investigation of Thin SiO_x and SiO_xN_y Overlayers*", J. Molecular Science*, 480, 611-614, **1999**

[34] G. Johansson, J. Hednal, A. Berndtsson, M. Klasson, R. Nilsson, "Calibration of Electron Spectra", *J. Elec. Spec. Rel. Phen.*, 2, 295-317, **1973**

[35] R. J. Bird, P. Swift, "Energy Calibration in Electron Spectroscopy and Re-determination of Some Reference Electron Binding Energies", *J. Elec. Spec. Rel. Phen.*, 21(3), 227-240, **1980**

[36] S. Kohiki, T. Ohmura, K. Kusao, "A new Charge Correction Method in X-ray Photoelectron Spectroscopy", *J. Elec. Spec. Rel. Phen.*, 28(4), 229-238, **1983**

[37] S. Kohiki, T. Ohmura, K. Kusao, "Appraisal of a new Charge Correction Method in X-ray Photoelectron Spectroscopy", *J. Elec. Spec. Rel. Phen.*, 31(1), 85-90, **1983**

[38] M. P. Seah, I. S. Gilmore, G. Beamson, *Surf. Interface Anal.*, 26, 642-649, **1998**

[39] C. D. Wagner, A. Joshi, "The Auger Parameter, Its Utility and Advantages: A Review", *J. Elec. Spec. Rel. Phen.*, 47, 283-313, **1988**

[40] G. K. Wertheim, S. B. Dicenzo, S. E. Youngquist, "Unit Charge on Supported Gold Clusters in Photoemission Final State", *Phys. Rev. Lett.*, 5(25), 2310-2313, **1983**

[41] T. L. Barr, "Studies in Differential Charging", *J. Vac. Sci. Technol. A*, 7(3), 1677-1683, **1989**

[42] T. Dickinson, A. F. Povey, P. M. A. Sherwood, "Differential Sample Charging in ESCA", *J. Elec. Spec. Rel. Phen.*, 2, 441-447, **1973**

[43] J. B. Metson, "Charge Compensation and Binding Energy Referencing in XPS Analysis", *Surf. Ineterface Anal.*, 27, 1069-1072, **1999**

[44] J. Cazaux, "Mechanisms of Charging in Electron Spectroscopy", *J. Elec. Spec. Rel. Phen.*,105, 155-185, **1999**

[45] W. M. Lau, "Use of Surface Charging in X-ray Photoelectron Spectroscopy Studies of Ultrathin Dielectric Films on Semiconductors", *Appl. Phys. Lett.*, 54(4), 338-340, **1989**

[46] J. H. Thomas, C. E. Bryson, T. R. Rampalone, "X-ray Photoelectron Spectroscopy Surface Charge Buildup Used to Study Residue in Deep Features on Integrated Circuits", *J. Vac. Sci. Technol. B*, 6(4) 1081-1086, **1988**

[47] H. Doron-mor, A. Hatzor, A. Vaskevich, T. Van der Boom-Moav, A. Shanzer, I. Rubinstein, H. Cohen, "Controlled Surface Charging as a Depth-profiling Probe for Mesoscopic Layers", *Nature*, 406, 382-385, **2000**

[48] A. Cros, "Charging Effects in X-ray Photoelectron Spectroscopy", *J. Elec. Spec. Rel. Phen.*, 59, 1-14, **1992**

[49] N. J. Havercroft, P. M. A. Sherwood, "Use of Differential Surface Charging to Separate Chemical Differences in X-ray Photoelectron Spectroscopy", *Surf. Interface Anal.*, 29, 232-240, **2000**

[50] A. Barranco, F. Yubera, J. P. Espinos, A. R. Gonzales-Elippe, Surf. Interface Anal., 31, 761, **2001**

[51] C. D. Wagner, A. J. Joshi, J. Elec. Spec. Rel. Phen., 47, 283**, 1988**

[52] C. D. Wagner, Anal. Chem., 44, 972, **1972**

[53] L. Magagnin, R. Maboudian, C. Carraro, "Gold Deposition by Galvanic Displacement on Semiconductor Surfaces: Effect of Substrate on Adhesion", *J. Phys. Chem. B*, 106, 401-407, **2002**

[54] X. Cheng, G. Li, E. A. Kneer, B. Vermiere, H. G. Parks, S. Raghavan, J. S. Jeon, *J. Electrochem. Soc*., 145(1), 352-357, **1998**

[55] A. Sargent, O. A. Sadik, "Impedance and Morphological Properties of Electroless Gold on Industrial Metal Coupons", *Langmuir*, 17, 2760-2767, **2001**

[56] M. C. Barnes, Doh-Y. Kim, Hyo S. Ahn, C. O. Lee, N. M. Hwang, "Deposition Mechanism of Gold by Thermal Evaporation: Approach by Charged Cluster Model", *J. Cryst. Growth*, 213, 83-92, **2000**

[57] H. Nagata, T. Shinriki, K. Shima, M. Tamai, E. M. Haga, "Improvement of Bonding Strength Between Au/Ti and SiO_2 Films by Si Layer Insertion", *J. Vac. Sci. Technol. A*, 17(3), 1018-1023, **1999**

[58] J. A. DeRose, D. B. Lampner, S. M. Lindsay, N. J. Tao, "Comparative Scanning Probe Microscopy Study of the Surface Morphology of Au Films Grown from the Vapor onto Glass, Fused Silica, and Muscotive Mica", *J. Vac. Sci. Technol. A*, 11(4), 776-780, **1993**

[59] Q. Guo, K. Luo, K. A. Davis, D. W. Goodman, "Initial Growth of Gold on Oxides", Surf. Interface Anal, 32, 161-165, **2001**

[60] K. Luo, D. Y. Kim, D. W. Goodman, "The Nucleation and Growth of Gold on Silica", *J. Molec. Catal. A: Chem*, 167, 191-198, **2001**

[61] S. Suzer, N. Ertas, S. Kumser, O. Y. Ataman, "X-ray Photoelectron Spectroscopic Characterization of Au Collected with Atom Trapping on Silica for Atomic Absorption Spectrometry", *Appl. Spec.*, 51(10), 1537-1539, **1997**

[62] S. Suzer, N. Ertas, O. Y. Ataman, "XPS Characterization of Bi and Mn Collected on Atom-Trapping Silica for AAS", *Appl. Spec.*, 53(4), 479-482, **1999**

[63] S. Suzer, "Deposition and Stability of Metal Ions on Oxidised Silicon Surfaces: Electrohemical Correlation", *J. Elec. Spec. Rel. Phen*, 114-116, 1151-1154, **2001**

[64] S. Suzer, O. Dag, *Can. J. Chem.*, 78, 516-519, **2000**

[65] G. Rubio, N. Agrait, and S. Vieira, 'Atomic-Sized Metallic Contacts: Mechanical Properties and Electronic Transport', Phys. Rev. Lett., 76(13), 2302-2305, **1996**

[66] J. Turkevich, P. C. Stevenson, J. Hillier, *Faraday Discussions Chemical Society,* 11, 55, **1951**

[67] S. Biggs, M. K. Chow, C. F. Zukowski, F. Grieser,"The Role of Colloidal Stability in the Formation of Gold Sols" *Journal of Colloid and Interface Science*, 160, 511-513, **1993**

[68] S. L. Cumberland, F. Strouse, "Analysis of the Nature of Oxyanion Adsorption on Gold Nanomaterial Surfaces", Phys. Langmuir, 18, 269-276, **2002**

[69] S. R. Hall, W. Shenton, H. Engelhardt, S. Mann, "Site-specific organization of gold nanoparticles by biomolecular templating", *Chemphyschem*, 2 (No.3), 184-186, **2001**

[70] M. M. Alvarez, J. T. Khoury, T. G. Schaaff, M. N. Shafigullin, I. Vezmar, R. L. Whetten, "Optical Absorption Spectra of nanocrystal Gold Molecules", *J. Phys. Chem. B*, 101, 3706-3712. **1997**

[71] P. V. Kamat, "Photophysical, Photochemical and Photocatalytic Aspects of Metal Nanoparticles", *J. Phys. Chem. B*, 106, 7729-7744, **2002**

[72] A. Taleb, C. Petit, M. P. Pileni, "Optical Properties of Self-assembled 2D and 3D Superlattices of Silver Nanoparticles", *J. Phys. Chem B*, 12, 2214-2220, **1998**

[73] A. N. Shipway, M. Lahav, R. Gabai, I. Willner, "Investigations into the Electrostatically Induced Aggregation of Au Nanoparticles", Langmuir, 16, 8789-8795, **2000**

[74] F. Mafune, J. Kohno, Y. Takeda, T. Kondow, "Dissociation and Aggregation of Gold Nanoparticles under Laser Irradiation", J. Phys. Chem. B, 105, 9050-9056, **2001**

[75] B. Sadtler, A. Wei, "Spherical Ensembles of Gold Nanoparticles on Silica: Alectrostatic and Size Effects", Chem. Comm., 1993-1995, **2002**

[76] T. Sato, D. G. Hasko, H. Ahmed, "Nanoscale Gold Particles: Monolayer Organisation and Patterning", J. Vac. Sci. Technol. B, 15(1), 45-48, **1997**

[77] M. G. Mason, "Electronic Structure of Supported Small Metal Clusters", *Phys. Rev. B*, 27 (2), **1983**

[78] T. Ohgi, D. Fujita, "Consistent Size Dependency of Core-level Binding Energy Shifts and Single-electron Tunneling Effects in Supported Gold Nanoclusters", *Phys. Rev. B*, 66, 115410, **2002**

[79] V. W. Ballarotto, M. Breban, K. Siegrist, R. J. Phaneuf, and E. D. Williams, "Photoelectron emission microscopy of ultrathin oxide covered devices", *J. Vac. Sci. B*, 26(6), 2514-2518, **2002**

[80] C. J. Powell, A. Jablonski, "Electron effective attenuation lengths for applications in Auger electron spectroscopy and x-ray photoelectron spectroscopy", *Surf. Interface Anal.*, 33, 211-229, **2002**